X-ray transition radiation and its use in experiments

A. G. Oganesyan

Erevan Physics Institute, Erevan

Fiz. Elem. Chastits At. Yadra **16**, 137–182 (January–February 1985)

The basic characteristics of x-ray transition radiation (XTR) are considered; work on the experimental investigation of various types of XTR detector is reviewed. Physics experiments that use such detectors are analyzed. Some recommendations helpful in the development of such detectors are given.

INTRODUCTION

In the seventies, experimental technology—and with it the physics of high-energy particles—crossed the 100-GeV energy barrier. In the next years, energies above 1000 GeV will begin to be mastered. Some experiments have already begun at these energies with cosmic rays. The quantitative growth in the particle energy has brought with it a qualitative review of the methods of detection and, what is most important, identification of particles. At energies $\lesssim 100$ GeV, the traditional methods of particle identification—time-of-flight, measurements of the ionization in the region of its relativistic rise, Cherenkov counters, etc.,—have proved themselves splendidly. However, already at energies above 100 GeV the first two methods are effectively useless, and Cherenkov counters are transformed into very cumbersome pieces of equipment. For example, merely to eliminate an effect of diffraction on the resolution in differential Cherenkov counters, the condition $l \gg \lambda\beta/\Delta\beta$, where l is the length of the radiator and λ is the wavelength, must be satisfied.[1] In threshold Cherenkov counters used to distinguish particles with masses $m_1 < m_2$, the number of photons emitted per unit length is proportional to m_2^2/E^2, i.e., to ensure a definite particle detection efficiency the length of the counter must increase as E^2 and at energies > 100 GeV may be tens or hundreds of meters. It is obvious that at high energies the use of Cherenkov counters to identify particles is very problematic even in accelerator experiments with well focused and monoenergetic particle beams, to say nothing of cosmic-ray experiments.

Fundamentally new possibilities were opened up by the development in the methodology of experiments of x-ray transition-radiation detectors (XTR detectors). Numerous investigations showed that such detectors can identify particles up to values $\gamma = E/mc^2 \sim 10^4$–$10^5$ of the Lorentz factor. Confirmation of this follows from the dependence of the length of the various types of detectors designed for π/K and π/e identification on γ (Fig. 1)[2]—it is only the XTR detectors that can have a technically realizable length at these γ values. We do not have the possibility to dwell here on the numerous theoretical and experimental studies that have been made of the properties of this radiation. Those interested in these questions can consult the review of Refs. 3–9; a complete list of investigations during the period from the discovery of transition radiation up to 1982 can be found in Ref. 10.

We review here experimental work related to the investigation and development of XTR detectors. We give the main theoretical results needed for the design and planning of XTR detectors, and also the results of the most complete experimental studies of XTR properties. We analyze the principles of construction of the various XTR detectors, and we also describe experiments in which they have been used to identify particles.

Transition radiation, which was discovered by Frank and Ginzburg,[11] is like Cherenkov radiation in being the consequence of polarization of the medium and arises in the case of uniform motion of particles through a medium with permittivity $\varepsilon \neq 1$. However, in contrast to Cherenkov radiation, which arises only at particle velocities $v > c/\sqrt{\varepsilon}$, the condition for the generation of transition radiation is variability of ε along the direction of motion of the particles, or, and this is the same thing, variability of the phase velocity of the electromagnetic field which accompanies the particle. It was shown in Ref. 12 that the main fraction of the transition radiation that arises when an ultrarelativistic particle crosses an interface between two media with different permittivities is concentrated in the x-ray frequency region, where $\varepsilon = 1 - \sigma/\omega^2$ (here, $\sigma = 4\pi Ne^2/m$ is the square of the plasma frequency, N is the number of free electrons in 1 cm^{-3}, and m_e is the electron mass). The intensity of the radiation at the interface is determined by the difference between the radiation formation zones in the medium, Z_m, and in the vacuum, Z_v:

$$\frac{dW}{d\omega} = \frac{2e^2\omega^2}{\pi^3 c^3}(Z_m - Z_v)^2\,\theta^3\,d\theta, \tag{1}$$

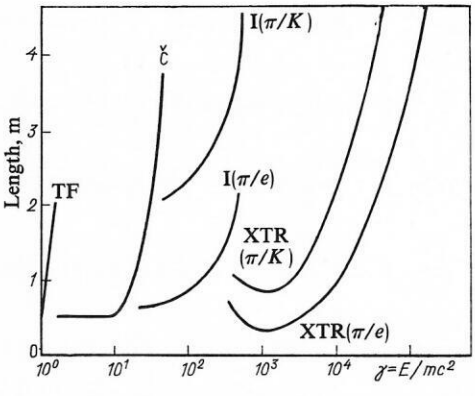

FIG. 1. Dependence of the length of different detectors on the Lorentz factor of the particles (TF, time-of-flight device; Č, Cherenkov counter; I, multiple measurement of ionization losses; XTR, transition-radiation detector).

 0090-4759/85/010060-21$04.40

where ω is the frequency of the radiation, θ is the angle between the direction of emission and the velocity of the particle, and

$$Z_m = \frac{\pi c}{\omega(\gamma^{-2}+\sigma/\omega^2+\theta^2)}; \quad (2)$$

$$Z_v = \frac{\pi c}{\omega(\gamma^{-2}+\theta^2)}. \quad (3)$$

The total radiation intensity

$$W = \frac{e^2\sqrt{\sigma}\,\gamma}{3\pi} \quad (4)$$

at one interface increases linearly with the Lorentz factor γ.

The radiation intensity in the case when a particle passes through a plate of thickness a is given by

$$\frac{d^2W}{d\omega\,d\theta} = \frac{2e^2\theta^3}{\pi c}(Z_m - Z_v)^2\left[4\sin^2\frac{b}{4Z_m}\right]. \quad (5)$$

As follows from (5), the radiation intensity in the case $a \gg Z_m$ is twice the intensity corresponding to one interface.

As follows from (1) and (5), the probability for emission of a transition-radiation photon, $dN/d\omega = (1/\hbar\omega)(Wd/d\omega)$, is very small. To enhance the radiation intensity, stacks of plates are used. An exact expression for the transition-radiation intensity in a stack consisting of n plates separated from each other by a distance b was derived with allowance for absorption of the radiation in the medium in Ref. 13. In the cases when the absorption in one plate is small [i.e., $a\mu(\omega) \ll 1$, where μ is the coefficient of absorption of the radiation in the medium], i.e., the effective number of plates is

$$n(\omega) = \frac{1-\exp(-\mu an)}{1-\exp(-\mu a)} \gg 1, \quad (6)$$

the spectral distribution of the transition-radiation intensity in the stack of plates can be represented in the form[6,14]

$$\frac{dW}{d\omega} = \frac{8e^2 n(\omega)}{\pi c}\sum_{r=r_{\min}}\left[2r - \left(\frac{\pi a}{Z_m(0)} + \frac{\pi b}{Z_v(0)}\right)\right] \times \left(\frac{1}{2r+Ab} - \frac{1}{2r+Aa}\right)^2 \sin^2\left[\frac{2\pi}{1+\alpha}(2r+Ab)\right], \quad (7)$$

where $\alpha = b/a$, $A = \sigma/(2\pi c\omega)$, $Z_m(0)$ and $Z_v(0)$ are the radiation formation zones for $\theta = 0$ in the medium and in the vacuum, respectively, and $r_{\min}$ is defined as the next larger integer for

$$r_{\min} = \frac{1}{2}\left(\frac{\pi a}{Z_m(0)} + \frac{\pi b}{Z_v(0)}\right). \quad (8)$$

A detailed analysis of XTR theory in a stack of plates is given in Refs. 15 and 16, which include the block diagram of an algorithm for calculating the intensity. We give here the characteristic features of this radiation, for which we introduce the notation

$$\gamma_0 = a\sqrt{\sigma}/2c = 25340a\sqrt{\sigma}, \quad (9)$$

$$\omega_0 = a\sigma/2c = 25340a\sigma, \quad (10)$$

where a is measured in centimeters, and ω_0 and $\sqrt{\sigma}$ in electron volts.

If no allowance is made for absorption of the radiation in the radiator itself, the following features of transition radiation can be identified:

1) for any ratio γ/γ_0, the radiation intensity decreases rapidly at frequencies $\omega > \omega_0$;

2) for $\gamma > 0.5\gamma_0$, the spectral distribution of the radiation contains a number of maxima at

$$\omega = \omega_0/(2s+1) \quad (s = 1, 2, 3 \ldots), \quad (11)$$

the main peak being at $\omega = \omega_0/3$ ($s = 1$);

3) for $\gamma > 0.5\gamma_0$ and $\omega = 0.18\omega_0$, there is a pronounced minimum in the radiation spectrum;

4) for $\gamma < 0.5\gamma_0$, the radiation intensity is low; with increasing γ, it increases rapidly up to $\gamma \approx 2\gamma_0$; with further increase in γ, the intensity increases logarithmically if $\alpha \gg 1$ or if the stack of plates is in a vacuum, and it tends to an asymptotic value at $\gamma \approx 10\gamma_0$ if α is not very large or if the stack of plates is in a gas.

1. EXPERIMENTAL INVESTIGATION OF THE PROPERTIES OF X-RAY TRANSITION RADIATION

The overwhelming majority of experimental studies so far made have been devoted to the investigation of various forms of XTR detectors. Detailed investigation of characteristics such as the spectral distribution of the radiation, the dependence of the positions of the interference maxima on the radiator parameters, etc., has been made in comparatively few studies.[17–27] A difficulty in such measurements is that it is necessary to detect separately the radiation and the particle, eliminating at the same time the possible simultaneous detection of two or more XTR photons. In addition, the radiation detector must have a high resolution, permitting the determination of the interference maxima and minima in the spectral distribution. These conditions were best met in the investigations of Refs. 24 and 27, in which a single-crystal Bragg spectrometer was used to measure in the interval $4 \leqslant \hbar\omega \lesssim 30$ keV the spectral distribution of the transition radiation of electrons with energies 5 and 9 GeV. The arrangement of the experiment is shown in Fig. 2. The XTR radiator consisted of 200–1000 layers of polypropylene (CH_2) of thickness $a = 16$–82 μm with air gaps of $b = 1.4$ mm. The electrons were deflected by the magnet and then detected by a system of scintillation counters, while the XTR photons, having passed through the collimator, were scattered in the crystal and detected by a proportional counter. Figure 3 shows the experimentally measured spectral distributions of the transition radiation in three different radiators. The number of layers in each of them is chosen to make the total amount of matter and, therefore, the absorptive capacity of the radiator and the multiple scattering of the electrons stay unchanged. Figure 3 also shows theoretical spectra with allowance for absorption of the radiation in the radiator. It can be seen that with increasing thickness of the layer the radiation spectrum becomes harder, in agreement with the theory; the positions of the interference maxima and minima also correspond to the theory. However, the measured radiation intensity was 15–20% below the theoretical value. A possible reason for this given in Ref. 27 is incorrect allowance for absorption of the photons in the matter of the radiator. But it could have been due to the angular discrimination of the radiation, which was unavoidable for the configuration of the experiment.

In Ref. 27, an NaI scintillator of thickness 0.37 mm,

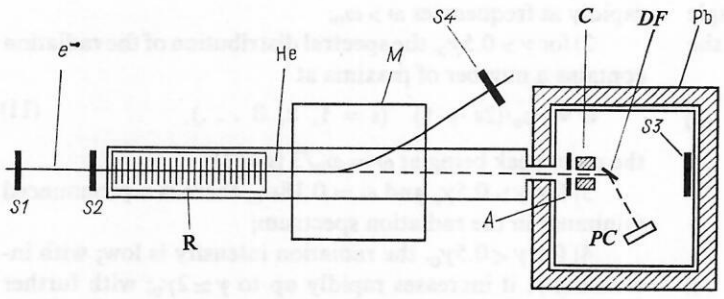

FIG. 2. Arrangement of the experiment of Ref. 24: S, scintillation counters; R, radiator; He, helium beam guide; M, bending magnet; A. anticoincidence counter; C, collimator; DF diffraction crystal; PC, proportional counter; Pb, lead screen.

instead of a Bragg spectrometer, was also used in a series of measurements in order to have a wider interval of frequencies. Measurements were made in two different polypropylene radiators ($n = 200$, $a = 244$ μm, $b = 0.75$ cm and $n = 100$, $a = 244$ μm, $b = 1.5$ cm) for 6.4-GeV electrons. Figure 4 shows the spectra of the transition radiation in each of the radiators as measured experimentally (histograms) and calculated by the Monte Carlo method (continuous curve). Although the resolution of the NaI scintillator was worse than for the Bragg spectrometer, the agreement between theory and experiment in this case is obvious. One can see fairly clearly interference maxima at 28 and 17 keV, which correspond to $s = 2$ and $s = 3$ [see (11)]. However, the main maximum at $s = 1$ ($\hbar\omega = 86$ keV) is not observed; according to Cherry,[27] this is due to the fact that the condition $\gamma > 0.5\gamma_0$ was satisfied weakly. However, in our view, a not unimportant factor here was the low radiation-detection efficiency (about 25% at $\hbar\omega = 86$ keV) and the poor resolution (about 30%) of the NaI scintillator, and also the detection of two or more simultaneously emitted photons.

It is of interest to investigate XTR in radiators made of copper[28] and tin[29] foil. The aim of the quoted studies was to

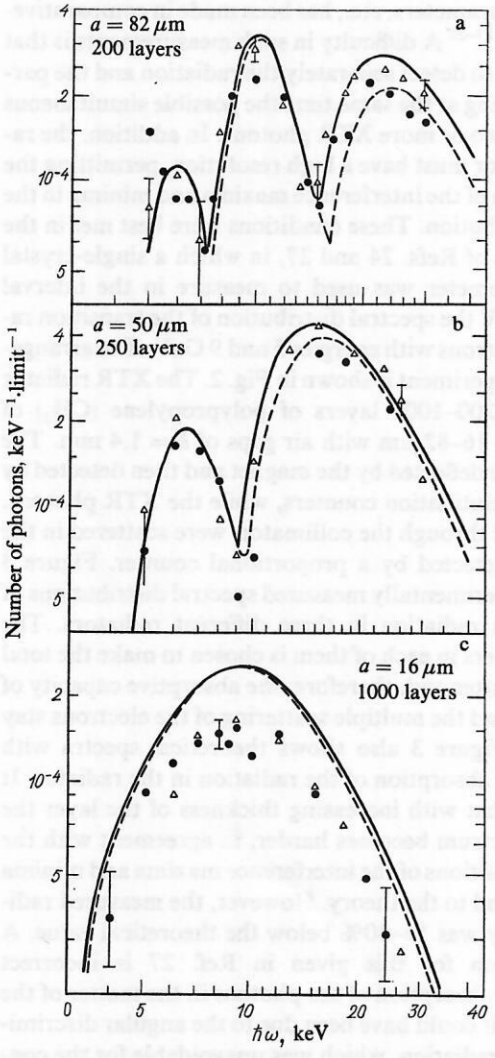

FIG. 3. Spectrum of the transition radiation of electrons in different radiators. The open triangles and the continuous curves correspond to $E = 9$ GeV; the black circles and the broken curves, to $E = 5$ GeV.

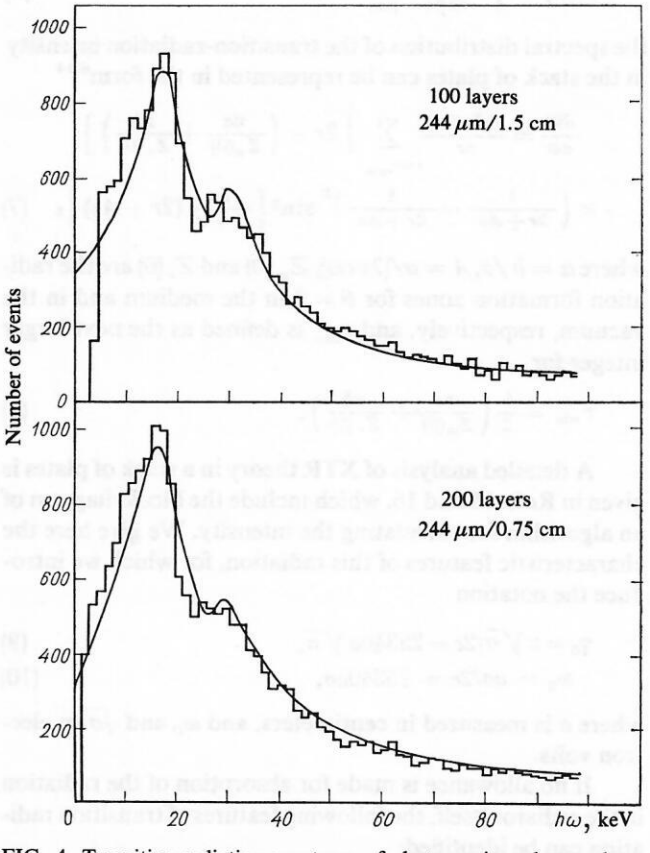

FIG. 4. Transition-radiation spectrum of electrons in polypropylene, measured by an NaI scintillator.

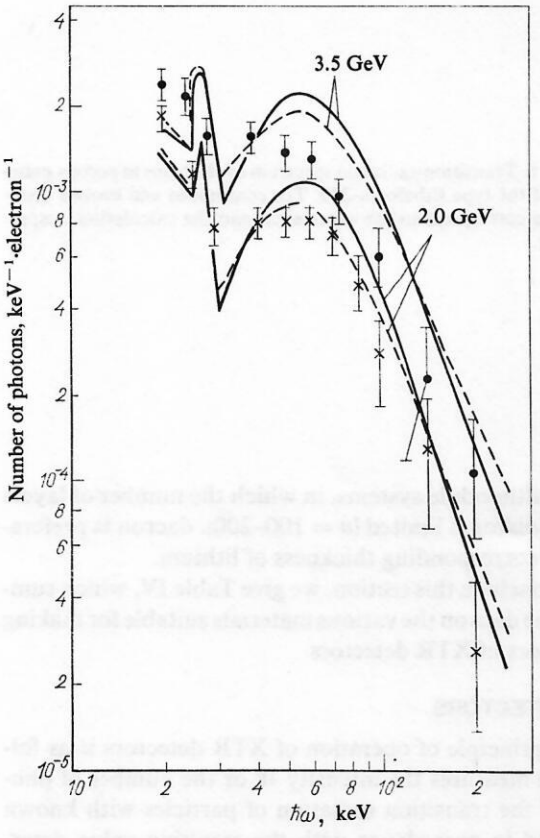

FIG. 5. Transition-radiation spectra of electrons in tin foils. The black circles and crosses correspond to 3.5 and 2.0 GeV, respectively; the continuous and broken curves, to the calculation with and without allowance for multiple scattering of the electrons, respectively.

investigate the effect of multiple electron scattering on the mechanism of formation of the transition radiation. In particular, a study was made in Ref. 29 in the range 20–200 keV of the spectrum of transition radiation produced by the passage of 1.0–3.5-GeV electrons through a radiator consisting of 20 tin foils of thickness 20 μm, separated by spaces of 1 mm; the radiation was detected by an NaI scintillator. Figure 5 shows the XTR spectra. According to the authors, the experimental results in the region $40 \leqslant \hbar\omega \leqslant 100$ keV agree better with the calculations that take into account multiple scattering. These measurements, and also the theoretical studies of Refs. 30–32, indicate that at $\gamma \leqslant 10^6$ multiple scattering in the region $\hbar\omega \lesssim 100$ keV does not significantly affect the integrated XTR intensity.

From the point of view of the construction of economic XTR detectors, transition radiation in irregular (porous) media is of great interest. The use of plastic foam as a radiator was proposed for the first time in Ref. 33. Since then, numerous investigations into the properties of such radiators have been made.[34–39] A theory of transition radiation in irregular media was developed in Refs. 40 and 41. Here, we consider the results of Refs. 36 and 38, in which a detailed study was made of various porous materials and a comparison was made with both theory and periodic radiators.

In Ref. 38. a semiconductor detector was used to investigate the XTR spectral distribution at electron energy 1.38 GeV in different porous materials of length 5 cm, the characteristics of which are given in Table I. Figure 6 shows the spectral distribution for one of the radiators (Ethafoam-220). Also shown is the calculated distribution obtained on the basis of Refs. 40 and 41. Table I gives the measured and calculated values of the mean energy and number of XTR photons in three different materials. As follows from Fig. 6 and Table I, the theoretical values agree well with the experiment, provided the mean pore radii and the thickness of the walls between the pores are correctly determined.

In Ref. 36, a comparison was made of the energy deposition of electrons in 4 cm of xenon and krypton in a periodic stack of mylar plates ($a = 25\,\mu$m, $b = 1.5$ mm, $n = 188$) and different porous materials of thickness 4 cm at energy 9 GeV. The parameters of these materials, and also the results of the comparison, are given in Table II. It is obvious that the comparison is somewhat arbitrary in nature, since for other thicknesses of the gases and radiators the ratios of the XTR intensity and the radiation losses could be different. Nevertheless, it follows from Table II that the radiation capacities of the different porous materials differ strongly; this is due not only to the differences between the densities, pore sizes, and wall thicknesses but, in the first place, also to the chemical composition, i.e., the absorbing capacity of the radiator material.

A radiator made of lithium hydride (LiH) powder was investigated for the first time in Ref. 37. In Ref. 38, such a radiator was optimized by a calculation. Table III gives the dependences of the number of photons and the energy W_p absorbed in a xenon proportional chamber on γ for radiator densities equal to 5 and 10% of the density of continuous LiH. Comparison of Tables I and III shows that the porous LiH radiator has a very high radiation capacity even at small γ.

TABLE I. Dependence of the energy deposition W and number N of detected photons on the parameters of porous radiators.

Radiator	ρ, g/cm^3	$\bar{a}$, μm	$\bar{b}$, mm	Equivalent number of plates	$\bar{W}$, keV		N	
					Experiment	Calculation	Experiment	Calculation
Ethafoam-220	0.037	35±14	0.87±0.31	56	6.96	7.07	0.45	0.46
Ethafoam-400	0.053	44±17	0.70±0.34	71	7.81	8.14	0.49	0.51
Ethafoam-600	0.111	100±31	0.55±0.24	80	6.62	6.01	0.40	0.37

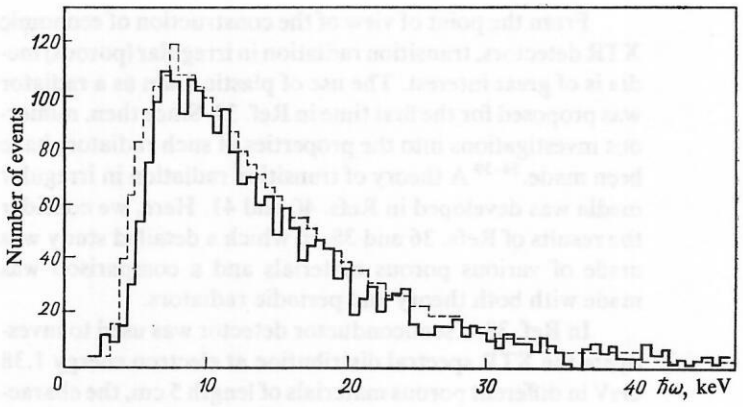

FIG. 6. Transition-radiation spectrum of electrons in porous material of the type Ethafoam-220. The continuous and broken histograms correspond to the experiment and the calculation, respectively.

It is obvious that the yield of the transition radiation depends to a large degree on the atomic number Z and on the density ρ of the radiator material. On the one hand, the higher ρ, the higher the plasma frequency $\sqrt{\sigma} = 28.8(Z\rho/A)^{1/2}$ and, therefore, the radiation intensity. But, on the other hand, with increasing ρ and, especially, Z the probability of absorption of the radiation in the radiator itself increases sharply. As a result, at large ρ and Z there is an effective yield of radiation only from the final layers of the radiator. To compare the radiation capacity of different radiators, we have calculated the numbers of photons emitted in one layer of liquid hydrogen, lithium, dacron, and aluminum. The thickness of the layer of each material was chosen to make the shape of the XTR spectral distribution the same in all cases. As follows from Fig. 7, which shows the corresponding spectral distributions, the radiation intensity in one plate (without allowance for absorption) is appreciably higher in the case of aluminum than for lithium. However, it can be seen from Fig. 8, which gives the number of photon in the interval $3 \leqslant \hbar\omega \leqslant 25$ keV at the end of different radiators as a function of the number of layers, that radiators with small values of ρ and Z have an undisputable advantage. It is for this reason that in XTR radiators one is recommended to use materials such as lithium or hydrocarbon polymers (for technical reasons, liquid hydrogen and beryllium are impracticable; in addition, the latter is decidedly toxic). Note that in multimodule systems, in which the number of layers in each radiator is limited ($n = 100$–200), dacron is preferable to the corresponding thickness of lithium.

To conclude this section, we give Table IV, which summarizes the data on the various materials suitable for making the radiators of XTR detectors.

2. XTR DETECTORS

The principle of operation of XTR detectors is as follows. One measures the intensity W or the number of photons N of the transition radiation of particles with known energy and in accordance with the resulting value determines the Lorentz factor γ of the radiating particle. However, since the transition radiation is emitted at very small angles with respect to the direction of motion of the particles, the separate detection of the photons and the particle itself presents some difficulties. The following ways are known for solving this problem: the energy-deposition method, separation of the particle from the radiation in the field of a bending magnet, the method of the characteristic radiation and (or) Compton scattering, the method of angular discrimination, and the visual method (using a streamer chamber). Of these, the first method is based on the difference in energy between the particle and the radiation, while the remainder are based on their spatial separation. So far, only XTR detectors based on the energy-deposition method

TABLE II. Radiation capacity of the different porous radiators.

Radiator	ρ, g/cm^3	(dE/dx)/ (XTR)	
		Kr	Xe
Mylar	0.02	0.9	0.9
Ethafoam polyurethane	0.03	0.8	0.7
Astrobubbles SP 423	0.03	0.6	0.6
Styrofoam DB	0.03	0.5	—
Eccospheres EP 100	0.10	0.5	0.3
Dorvon FR 100	0.01	0.4	0.3
Styrofoam HD 300	0.05	0.4	0.2
Styrofoam SI	0.04	0.3	—
Styrofoam FR	0.02	0.3	0.3
Polyurethane (18 Pores/cm)	0.03	0.3	—
Styrofoam SM	0.03	0.3	0.2
Loeperm Polyurethane LP1A	0.02	0.2	0.2
Polyurethane (12 Pores/cm)	0.03	0.2	—

TABLE III. Dependence of the energy deposition W_p and the number N_p of detected photons on γ in a radiator of LiH powder.

γ	Diameter of granules, μm	Thickness of multiwire proportional chamber, cm	5 % *		10 % **	
			$\bar{W}_p$, keV	$\bar{N}_p$	$\bar{W}_p$, keV	$\bar{N}_p$
200	4.0	0.2	0.88	0.27	0.77	0.24
400	6.0	0.4	4.92	1.19	4.43	1.06
600	8.0	0.4	9.44	2.04	8.27	1.75
1000	16.0	0.4	17.85	3.11	16.40	2.86

* $n = 2000$, $\bar{b}/\bar{a} = 12.0$.
** $n = 2000$, $\bar{b}/\bar{a} = 5.5$.

and the use of bending magnets have found practical application.

Energy-deposition method

The idea of the energy-deposition method, which was proposed for the first time in Ref. 42, is as follows. The charged particle in the company of the XTR photons enters the radiation detector after it leaves the radiator. In the detector, an energy W_Σ is deposited by both the ionization W_i produced by the particle and the absorption of XTR photons (W_a). Although at ultrarelativistic energies the ionization losses of the particles are almost independent of W_Σ, the energy W_a depends on γ, so that the energy depositions of particles with masses $m_1 < m_2$ at a given energy satisfy $W_{\Sigma 1} > W_{\Sigma 2}$, since $W_{a1} > W_{a2}$. Knowing the theoretical or experimental dependence of W_Σ on γ, one can determine the mass of the particle responsible for the energy deposition in the radiation detector. The latter is usually a multiwire proportional chamber filled with a large-Z gas, this making it possible for a relatively small value of W_i to ensure effective absorption of the XTR photons. Obviously, the larger the ratio W_a/W_i and the stronger the dependence of W_a on γ, the better the resolution of the XTR detector. Unfortunately, the problem of accurate identification of particles is complicated by the fact that both the ionization losses and the energy and number of XTR photons are subject to strong fluctuations. The fluctuations in W_i are determined by the Landau distribution and basically depend on the length l_g and the density ρ_g of the gas of the proportional chamber. The fluctuations in the number and energy of the XTR photons can be represented qualitatively in the form[43]

$$\sigma_N^2 = \int \frac{1}{\omega} \frac{dW_a}{d\omega} d\omega; \tag{12}$$

$$\sigma_W^2 = \int \omega \frac{dW_a}{d\omega} d\omega. \tag{13}$$

Characteristic W_Σ distributions at different electron energies[44] are shown in Fig. 9a. The arrows indicate the mean values $\bar{W}_\Sigma$. To decrease the fluctuations in the energy deposition and, therefore, improve the resolution of the XTR detector, one generally uses a number of modules consisting of radiators and multiwire proportional chambers arranged in a sequence. The narrowing of the distributions in a multimodule XTR detector is shown in Fig. 9b, which gives the results of Ref. 45. These distributions being available, the resolution is estimated as follows. Suppose these distributions correspond to particles 1 and 2 ($m_1 < m_2$). Then the percentage of particles 1 and 2 with energy deposition W

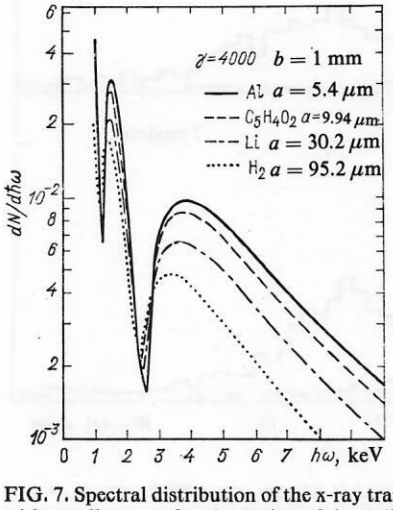

FIG. 7. Spectral distribution of the x-ray transition radiation in one plate without allowance for absorption of the radiation.

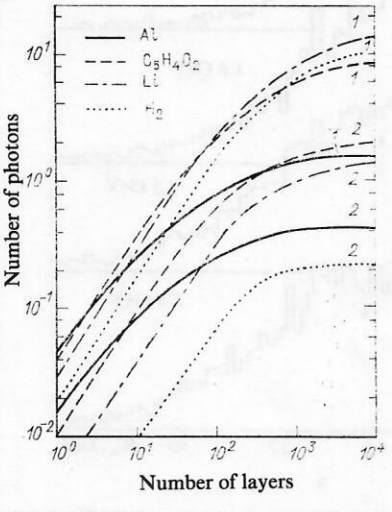

FIG. 8. Dependence of the number of transition x rays on the number of layers of different radiators: 1) $\gamma = 4000$; 2) $\gamma = 1000$.

TABLE IV. Properties of different materials used as XTR radiators.

Material	ρ, g/cm³	$\hbar\sqrt{\sigma}$, eV	$\left(\frac{\hbar\omega}{\gamma}\right)$, eV	$\left(\frac{Z_c}{\gamma}\right)$, cm	$\hbar\omega_k$, keV	Λ, cm	L_{rad}, cm	λ_{int}, g/cm²
H_2^*	0.071	7.9	5.6	$2.8\cdot10^{-6}$	2.8	36.3	887	55.4
Li	0.534	14.0	9.9	$1.6\cdot10^{-6}$	9.7	13.5	156	72.0
Be	1.848	25.8	18.2	$8.5\cdot10^{-7}$	13.6	1.35	35.7	76.0
Al	2.70	33.1	23.4	$6.6\cdot10^{-7}$	48.0	$1.4\cdot10^{-2}$	8.9	105
Fe	7.90	55.3	39.0	$4.0\cdot10^{-7}$	177	$7.1\cdot10^{-4}$	1.76	135
Cu	8.96	58.5	41.4	$3.8\cdot10^{-7}$	129	$5.0\cdot10^{-4}$	1.44	135
Sn	7.31	50.5	35.7	$4.3\cdot10^{-7}$	280	10^{-3}	1.22	170
W	19.3	80.3	56.8	$2.7\cdot10^{-7}$	445	$8.3\cdot10^{-4}$	0.35	194
Pb	11.3	61.0	43.1	$3.6\cdot10^{-7}$	535	$1.1\cdot10^{-3}$	0.56	208
LiH	0.82	19.1	13.5	$1.2\cdot10^{-6}$	8.9	—	113	—
Mylar ($C_5H_4O_2$)	1.38	24.4	17.3	$9\cdot10^{-7}$	20.0	0.124	28.7	73
Polyethylene (CH_2)	0.92	18.6	13.2	$1.2\cdot10^{-6}$	19.3	0.65	49.0	57
C fiber	1.90	28.0	19.8	—	—	—	43.3	—

*For the liquid phase at 1 atm and the boiling point.

Note. $\hbar\omega/\gamma$ is the photon energy at which the formation zone in the medium at the given γ is maximal; Z_c/γ is the maximal formation zone in the medium at the given γ; $\hbar\omega_k$ is the photon energy at which the cross sections of Compton scattering and the photoelectric effect are equal; Λ is the photon absorption range at $\hbar\omega = 10$ keV; L_{rad} is the radiation unit of length; and λ_{int} is the proton inelastic interaction range at $P = 20$ GeV/c.

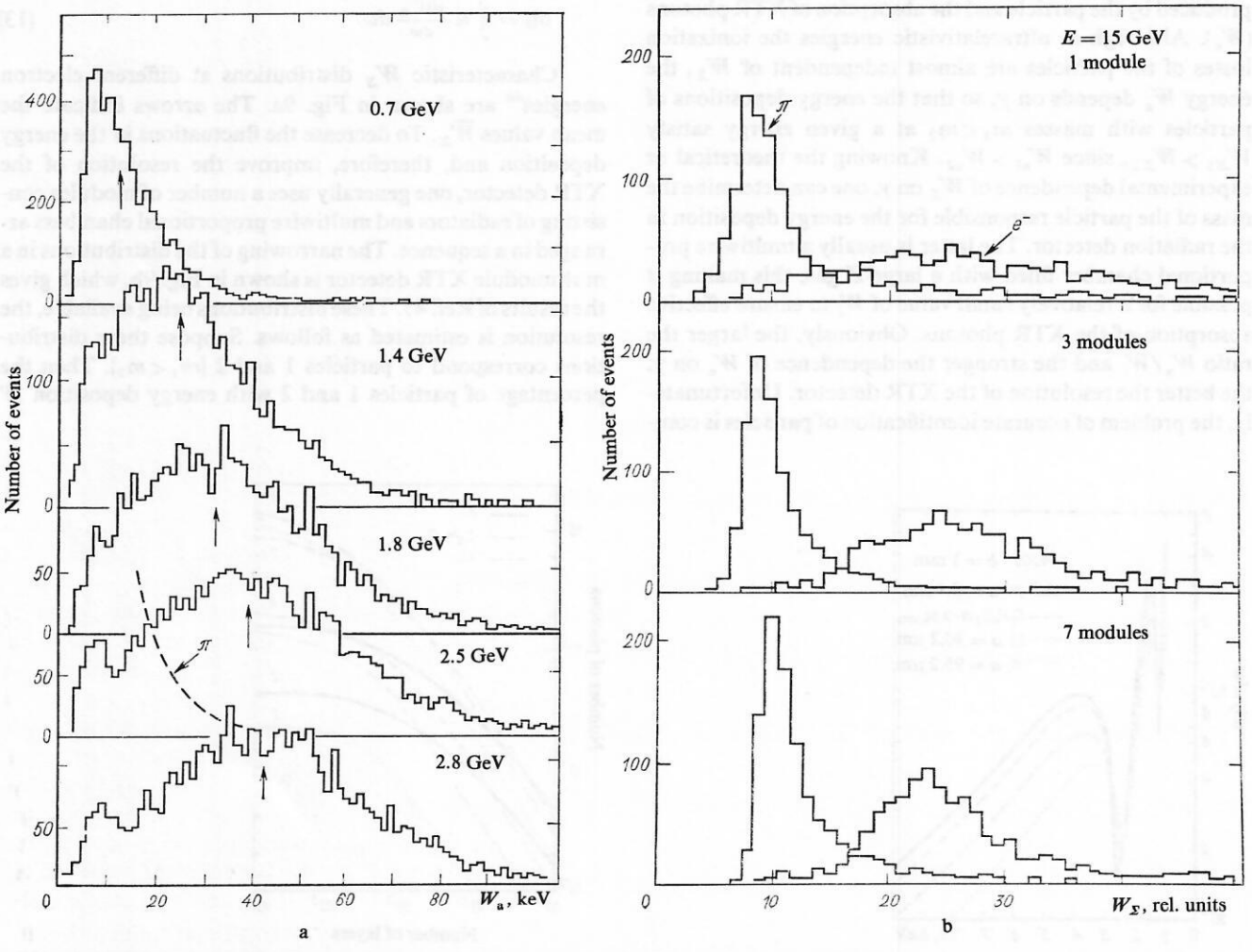

FIG. 9. Energy-deposition distributions: 1) for electrons of different energies[44] (lithium radiator, $a = 51$ μm, $b = 0.5$ mm, $n = 1000$ layers, $l_{Xe} = 1.04$ cm); b) for electrons and pions and different numbers of modules[45] (mylar, $a = 25$ μm, $b = 1.5$ mm, $n = 188$ layers, $l_{Xe} = 4$ cm).

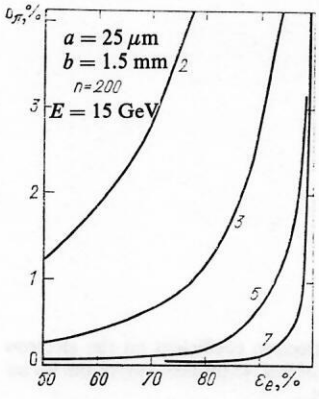

FIG. 10. Dependence of the pion rejection coefficient on the electron detection efficiency (the numbers next to the curves are the numbers of modules[45]).

exceeding the value W_{th}, where the two distributions intersect, characterizes the detection efficiency ε_1 for particles 1 and the rejection coefficient δ_2 for particles 2, respectively.

Similarly, for events with $W < W_{th}$ one determines the detection efficiency ε_2 for particles 2 and the rejection coefficient δ_1 for particles 1. However, the most accurate identification of particles in an m-module detector can be obtained by using the method of maximal likelihood.[45] Suppose there are exact forms of the energy-deposition distribution of particles 1 and 2 in each of the detector modules. After appropriate normalization, these distributions can be regarded as the probability distributions for particles 1 and 2 to produce the given signal in the given module. In passing through the detector, the identified particle produces a set of m values of the energy depositions W_i ($i = 1,2,...$). The value W_i in module i could be produced with probabilities $P_1^i(W)$ and $P_2^i(W)$ by particles 1 and 2, respectively. The probability that the given set was produced by particle 1 (or particle 2) is

$$P_{1,2} = \prod_{i=1}^{m} P_{1,2}^{i}(W). \tag{14}$$

Then the probability of interpreting the event as corresponding to the particles 1 and 2 is

$$R_{1,2} = P_{1,2}/(P_1 + P_2). \tag{15}$$

At the same time, the percentages of particles 1 and 2 with values R_1 and R_2 exceeding the given value R_1^{th} characterize the detection efficiency ε_1 and the rejection coefficient δ_2. Similarly, for $R_{1,2} < R_2^{th}$ we define δ_1 and ε_2. As an example, Fig. 10 gives the dependence of δ_π on ε_e obtained in Ref. 45 in an investigation of the separation of electrons from pions. The parameters of the XTR detector are given in Fig. 9b.

The fluctuations of the energy deposition depend to a large degree both on E and on the radiator parameters (a, b, n, the density ρ_r, and Z_r) and the gas of multiwire proportional chamber (l_g, Z_g, and ρ_g). As an illustration, let us consider the results of the experimental papers of Refs. 21 and 46. Figure 11a shows the dependence of the energy deposition on the distance between the layers or the radiator. It can be seen how the energy deposition tends to a plateau with increasing b; this means that the distance between the layers at the frequencies which make the main contribution to the energy deposition becomes equal in magnitude or greater than the radiation formation zone in vacuum. Figure 11b shows the dependence of the intensity of the transition radiation absorbed in a multiwire proportional chamber on the thickness of the radiator layer,[21] from which it follows that the choice of too small or too large a leads to a decrease in the energy deposition because of the suppression of the radiation formation or the increase in the radiation absorption in the detector itself, respectively. It is important to note that the optimal values of a and b depend both on γ and on the parameters of the proportional chamber. From this point of view, it is interesting to examine Fig. 12, which gives the

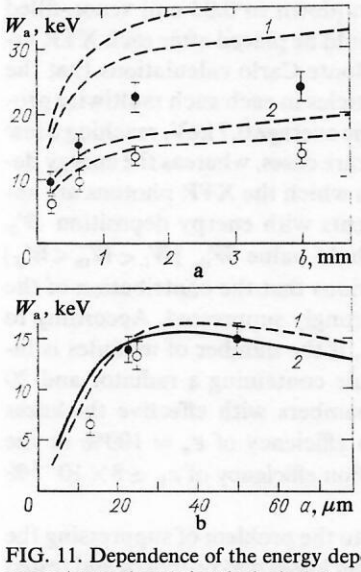

FIG. 11. Dependence of the energy deposition W_a: a) in a 4-cm layer of xenon (curve 1 and the black circles) and krypton (curve 2 and the open circles) on the distance b between the layers (mylar, $a = 25\ \mu m$, $n = 188$, $E = 15$ GeV; the regions between the broken curves represent corresponding calculations with allowance for uncertainties; b) on the thickness a of the layer of radiator (curve 1 and the black circles for polypropylene, curve 2 and the open circles for mylar; $b = 1.5$ mm, $n = 188$, $l_{Xe} = 4$ cm, $E = 10$ GeV).

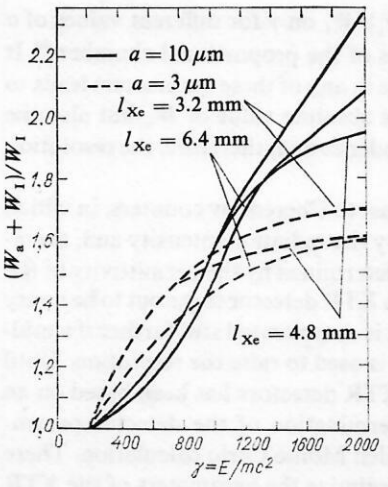

FIG. 12. Dependence of the ratio $(W_a + W_I)/W_I$ of the total energy deposition to the ionization loss on γ.[46]

dependence of $(W_a + W_i)/W_i$ on γ for different values of a and different thicknesses of the proportional chamber.[46] It can be seen how a change in any of these parameters leads to a change in not only the absolute value of W_a but also the shape of its energy dependence and, therefore, the resolution of the XTR detector.

Therefore, in contrast to Cherenkov counters, in which for given particle velocity the radiation intensity and, therefore, the resolution are determined by the permittivity of the radiator, the design of an XTR detector turns out to be a very complicated problem. It is complicated still further if a multimodule XTR detector is used to raise the resolution. Until recently, the design of XTR detectors has been based on an initial approximate determination of the detector parameters followed by a detailed Monte Carlo calculation. There have been attempts to optimize the parameters of the XTR detectors as well,[21,25,43,44] but these have all been approximate. They have not taken into account the number of layers of the radiator, the dependence of W_Σ on γ, the fluctuations in the energy deposition, and so forth. In Ref. 47, a method was proposed for designing XTR detectors which is free of these shortcomings and permits the achievement of the greatest possible resolution. The basic parameters are, as in any real experiment, the energy $E_1 = E_2$ of the identified particles with masses $m_1 < m_2$ and the admissible detector length L. Since the resolution of an XTR detector is higher, the larger the value of $W_{\Sigma 1} - W_{\Sigma 2} - \Delta W_{\Sigma 1} - \Delta W_{\Sigma 2}$, where $W_{\Sigma 1,2} = W_{a1,2} + W_{i1,2}$ and $\Delta W_{\Sigma 1,2} = [(\Delta W_{a1,2})^2 + (\Delta W'_{i1,2})^2]^{1/2}$ is the half-width of the distributions, variation of the variables is used to minimize

$$R = (\Delta W_{\Sigma 2} + \Delta W_{\Sigma 1})/(W_{\Sigma 1} - W_{\Sigma 2}). \qquad (16)$$

The smallest value of R corresponds to the optimal values of the mutually matched parameters of the radiator (a,b,n) and the thickness of the multiwire proportional chamber for the given number of modules and the chosen gas of the proportional chamber. Note that $W_{i1,2}$ can be determined from the well-known Bethe–Bloch formula, $\Delta W_{a1,2}$ can be calculated in accordance with (13), and known experimental values can be used for $\Delta W_{i1,2}$. To illustrate the scope of such optimization, Fig. 13 shows the pion rejection coefficient as a function of the electron detection efficiency obtained experimentally[45] for a three-module XTR detector with $a = 25\ \mu$m, $b = 1.5$ mm, $n = 188$, and $l_{Xe} = 4.3$ cm at energy 3 GeV. Also shown is the calculated dependence corresponding to the optimal values of a, b, n, and l_{Xe} for the same length of the XTR detector. It can be seen that the detector with the optimal parameters has a much higher resolution than was achieved in Ref. 45.

Development of the energy-deposition method

As can be seen from the above, the energy-deposition method gives an adequate resolution when the ionization produced by the XTR photons is appreciably greater than the ionization produced by the particle itself. It is therefore natural that the development of XTR detectors based on the energy-deposition method proceeded in the direction of a search for a method to suppress the ionization produced by the particle without a significant reduction in the number of detected XTR photons.

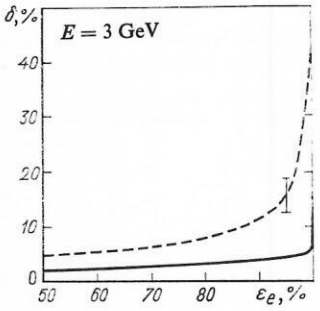

FIG. 13. Dependence of the pion rejection coefficient on the electron detection efficiency in the experiment of Ref. 45 (broken curve) and for an optimized detector (continuous curve).

Practically, the first step in this direction was made in Refs. 48 and 49, in which the layers of an XTR radiator of aluminized dacron of thickness 15 μm were simultaneously high-voltage electrodes of proportional chambers; the signal wires of diameter 20 μm were placed in the gaps between the layers. The radiator was placed in a space filled with a 90% Xe + 10% CO_2 mixture at pressure 2.6×10^{-2} atm (2.7×10^3 Pa). Lowering the pressure reduces the contribution of ionization losses to the total energy deposition and, therefore, improves the resolution of the XTR detector. The distributions of the energy depositions of pions and protons measured in one XTR-detector module consisting of 20 proportional chambers (i.e., 21 layers) connected together by a common load showed that if ten such modules are used, pions can be separated from protons with sufficient reliability at $E \gtrsim 100$ GeV.

The next step in suppressing the contributions of the ionization losses was made in Ref. 50, in which it was proposed that 10–20 very thin (down to 0.05 cm) xenon-filled proportional chambers should be placed after each XTR radiator. It was shown by Monte Carlo calculations that the ionization losses of the particles in each such multiwire proportional chamber are on the average 0.7 keV, reaching a few kilo-electron-volts only in rare cases, whereas the energy deposition in the chambers in which the XTR photons are absorbed is 3–20 keV. If events with enerpy deposition W_Σ exceeding the given threshold value W_{th} $(W_i < W_{th} \leqslant W_\Sigma)$ are discriminated, it is obvious that the contribution of the ionization losses will be strongly suppressed. According to the calculations of Ref. 52, if the number of modules is increased to five (each module containing a radiator and 20 multiwire proportional chambers with effective thickness 0.05 cm), a pion detection efficiency of $\varepsilon_\pi = 100\%$ at the same time as a kaon detection efficiency of $\varepsilon_K \approx 8\times10^{-3}\%$ can be achieved.

The simplest solution to the problem of suppressing the contribution of the ionization losses was proposed and tested experimentally by means of a device consisting of an XTR radiator and a drift chamber.[51,52] In this case, the charged particle produces on the average in the drift gap ionization that is uniformly distributed along the track, and the XTR photons produce local ionization clusters. If the time con-

TABLE V. Parameters of radiators used in Ref. 54.

Radiator	Plate thickness μm	Distances between plates, μm	Thickness of one radiator		Thickness of 12 modules		
			l, cm	l, g/cm^2	l, cm	l, g/cm^2	l, rad. units
Lithium	30	160±80	2.0	0.19	36	2.28	0.027
Lithium	35	240±80	4.5	0.30	66	3.60	0.043
Graphite fiber	7	—	4.5	0.30	66	3.60	0.09

stant of formation of the pulses RC is appreciably less than the collection time t_c of the primary electrons into the gas multiplication region, then in the presence in the drift gap of uniform ionization the pulse height at the chamber output will be appreciably reduced. But the pulses corresponding to local ionization will hardly be reduced at all, since in this case $\bar{t}_c \lesssim RC$.

At CERN, detailed investigations of an XTR detector based on the same principle were made,[53] and then a prototype detector was developed with a more original solution, in which the drift chamber was replaced by an ordinary multiwire proportional chamber.[54] In this case, the XTR detector consisted of 12 modules; the parameters of the radiators are given in Table V. The proportional chambers were filled with a 50% Xe + 50% CH_4 mixture and were 0.8-cm thick; at electron drift velocity $v^{-1} = 30$ nsec/mm in the multiwire proportional chamber, the total time of collection of the electrons from the track of the particle was 160 nsec. The current pulses produced by the local ionization in the chamber were amplified and shaped into a bell-shaped form with half-width 15 nsec, which corresponds to 500 μm in space. In the experiment, either the number of clusters with energy E_{cl} exceeding the threshold E_{th} of the discriminator was counted, or the part of the pulse current corresponding to a given section of length 1 mm of the track of the particle in the proportional chamber was analyzed by means of four analog-to-digital converters opened successively every 40 nsec for 40 nsec.

Figure 14a compares three methods of separating electrons from pions (Q is the usual energy-deposition method, ADC is the method of pulse-height analysis of the pulses from the four sections of the multiwire proportional chamber, and Disc is the method of counting the number of clusters with $E_{cl} \geqslant E_{th} = 4$ keV). It can be seen from Fig. 14a that the last method improves the resolution by 20–25 times compared with the traditional energy-deposition XTR detector. There is a similar improvement for all three radiators (see Table V). Figure 14b shows the dependence of the pion rejection coefficient in π/e separation on the total length and on the number of modules of the XTR detector, from which it follows that a detector consisting of 12 modules of length 65–75 cm can ensure a 1000-fold suppression of the pion number.

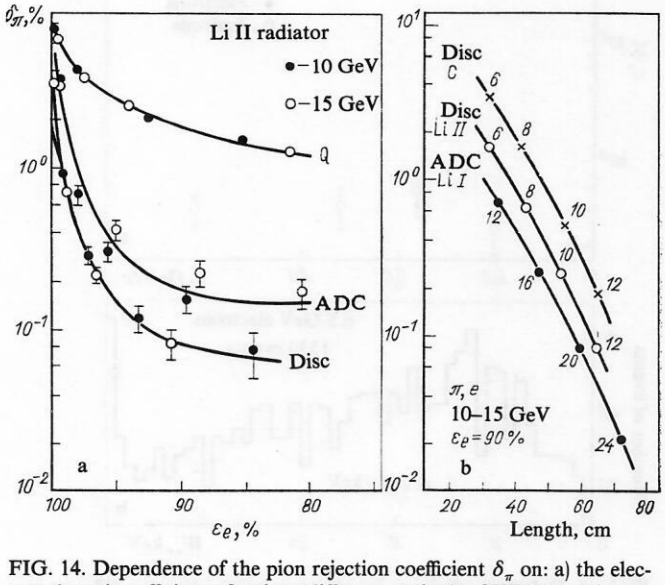

FIG. 14. Dependence of the pion rejection coefficient δ_π on: a) the electron detection efficiency for three different methods of XTR detection; b) the length of the XTR detector in the case of π/e identification. The numbers next to the curves are the numbers of modules.

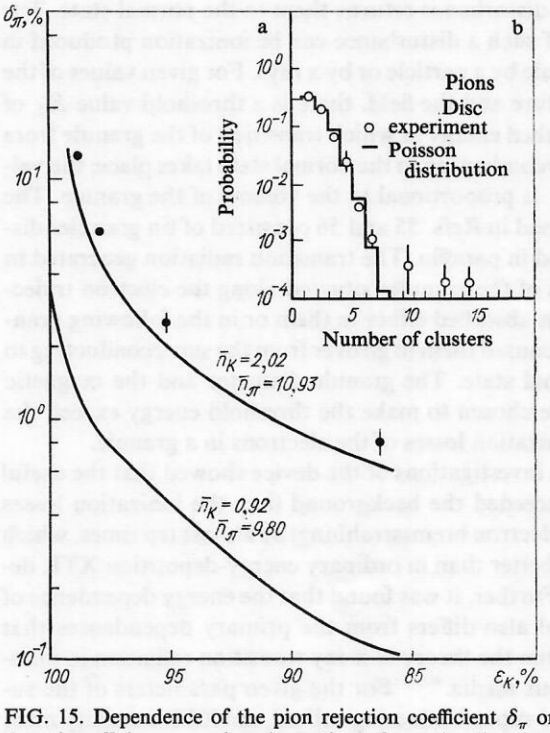

FIG. 15. Dependence of the pion rejection coefficient δ_π on the kaon detection efficiency ε_K when the method of counting the number of clusters is used (black circles and continuous curves[54]) (a) and distribution of the number of clusters due solely to ionization (b).[54]

Of interest here is Fig. 15a, which shows the pion rejection coefficient as a function of the efficiency of kaon detection bya 24-module XTR detector using the cluster-counting method (points). This dependence follows fairly well from the Poisson distributions for mean numbers of clusters $\bar{n}_K = 2.02$ and $\bar{n}_\pi = 10.93$ (continuous curve). However, as follows from analysis of Fig. 15b, which shows the probability distribution for formation of a given number of clusters by 15-GeV pions (i.e., when x-ray transition radiation is not formed), the mean number of clusters formed by δ electrons is $\bar{n}_\delta \simeq 1.1$. Therefore, in the case of Fig. 14a the number of clusters formed directly by XTR photons are $\bar{n}'_K \approx 0.9$ and $\bar{n}'_\pi \approx 9.8$, and if one could in some manner completely suppress the contribution of the δ electrons, the resolution would be improved still further. It is obvious that although a rise in the cluster detection threshold E_{th} does make it possible to reduce the value of $\bar{n}_\delta$, there is then to a considerable extent a decrease at the same time in the number of clusters produced by XTR photons and corresponding to the condition $E_{\text{cl}} \geqslant E_{\text{th}}$. As a result, the detector resolution only gets worse, as is indicated by the results of Ref. 54.

The device described in Refs. 55 and 56 can also be included in the class of XTR detectors based on the energy-deposition method. In it, a superheated superconducting colloid serves simultaneously as radiator and photon detector. The principle of operation of such a detector is as follows. In type-I superconducting metals (In, Sn, Ta, Pb, and Hg) in a field $H_{\text{cr}} < H < H_{\text{s}}$ there exists a superheated state, in which the metal is a superconductor (the critical field H_{cr} and the "superheating" field H_{s} are functions of the temperature). Such a metastable superconducting state can exist in spherical granules with diameter of a few microns until an external disturbance returns them to the normal state. The source of such a disturbance can be ionization produced in the granule by a particle or by x rays. For given values of the temperature and the field, there is a threshold value E_{th} of the absorbed energy at which transition of the granule from the superconducting to the normal state takes place; the value of E_{th} is proportional to the volume of the granule. The colloid used in Refs. 55 and 56 consisted of tin granules disseminated in paraffin. The transition radiation generated in the walls of the granules situated along the electron trajectories was absorbed either in them or in the following granules and caused them to go over from the superconducting to the normal state. The granule diameter and the magnetic field were chosen to make the threshold energy exceed the mean ionization losses of the electrons in a granule.

The investigations of the device showed that the useful signal exceeded the background (i.e., the ionization losses and the electron bremsstrahlung) by almost ten times, which is much better than in ordinary energy-deposition XTR detectors. Further, it was found that the energy dependence of the signal also differs from the primary dependences that follow from the theory of x-ray transition radiation in inhomogeneous media.[40,41] For the given parameters of the superheated superconducting colloid, the XTR intensity must reach a plateau value at $E > 2$ GeV; however, in the experiment a strong dependence of the signal on the electron energy was observed in this region. The authors of Refs. 55 and 56 attempted to explain this behavior of the energy dependence by the effect of multiple scattering on the formation of the x-ray transition radiation. But both theoretical[58] and experimental[28,29] study of this question showed that multiple scattering cannot lead to the results obtained in the experiment. Without doubting the results of the experiment, it seems to the present author that it is not justified to compare them with ordinary XTR theory. It is well known that the latter is valid if the point of observation of the radiation is sufficiently far from the point of its generation. In the case under consideration, this condition was not satisfied, since the radiation was already absorbed before it could be completely formed. It would appear that one should make a comparison of the experiment, not with the flux of radiated energy, but with the energy absorbed by the medium per unit time.

Methods using a bending magnet

It is obvious that complete elimination of the contribution of δ electrons without suppression of the transition radiation, i.e., the achievement of the maximal resolution in particle identification, can be achieved only by complete removal of the charged particle from the detector of the XTR photons, for example, by means of a deflecting magnetic field. As was noted above, bending magnets were used quite widely to investigate XTR characteristics. However, already in Ref. 59 a bending magnet was considered as an element of an XTR detector. A bending magnet of length 2 m was placed between a radiator consisting of 650 lithium foils of thickness 50 μm in a helium atmosphere and separat-

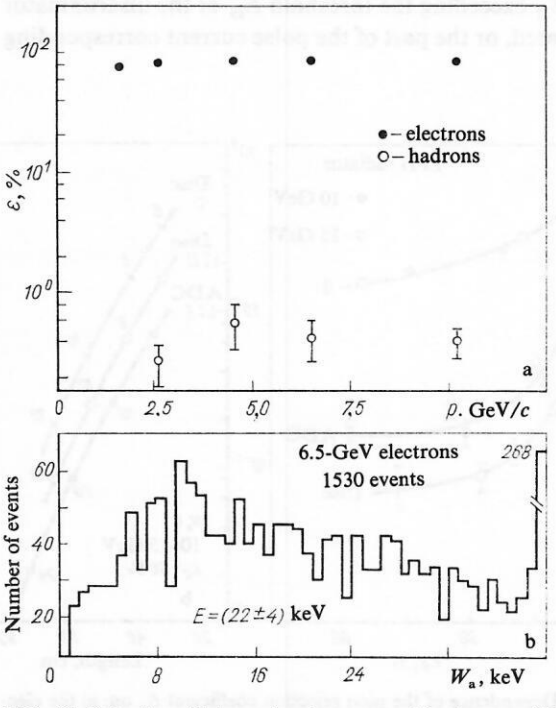

FIG. 16. Detection efficiency for electrons and hadrons at different momenta of the particles[59] (a) and distribution of the XTR energy deposition in the mutliwire proportional chambers (b).[59]

ed by 320 μm from each other and a proportional chamber (thickness 10 mm, 80% Xe + 20% CO_2 filling). For deflections of the particles through 40 mrad into a multiwire proportional chamber, the distance between the track of a particle and the region of absorption of the XTR photons was 6 cm. Investigations were made using beams of electrons and hadrons with momenta 1.6–10.2 GeV/c. At 2.6 GeV/c, an electron detection efficiency of about 8% (Fig. 16a) was achieved, the hadron detection efficiency being about 0.6%. The latter was largely due to random coincidences and to the detection of the products of the interaction of the hadrons with the lithium. As follows from Fig. 16b, which shows the distribution of the energy deposition of the XTR photons in the proportional chamber in the case of the detection of 6.5-GeV/c electrons, the mean detected energy is 22 keV. According to the estimate of the authors, just two XTR photons were detected on the average, this explaining the appreciable difference of the electron detection efficiency from 100%. Such an XTR detector (in conjunction with a single-module energy-deposition XTR detector) has been used in a beam of charged hyperons at CERN to investigate the Σ^-, Ξ^-, and Λ decay modes.[60] A spectrometric magnet, which in conjunction with drift chambers measures the momentum of the particles, plays the part of the bending magnet. According to Ref. 60, these XTR detectors make it possible to detect electrons with efficiency 83%, the rejection coefficient being 2.8×10^{-2}. We note that in Refs. 59 and 60 the parameters of the XTR detector were far from optimal.

A similar principle is the basis of the XTR detectors used at the Fermilab accelerator to identify pions[61,62] in a hadron beam consisting of pions, kaons, and protons in the ratio π:K:p = 300:10:1. Two magnets, which form part of the beam transportation system, are used as bending magnets. The radiators, placed in front of each of the magnets, consist of 1600 lithium foils of thickness 38 μm in a helium atmosphere with 800 μm between each of them. The radiation is detected by plastic Pilot B scintillators of thickness 10 cm. The plastic scintillator is chosen instead of the traditional multiwire proportional chambers because of the high intensity of the particle flux. However, in the case of a scintillator, fluctuations in the number of photoelectrons are added to the fluctuations in the XTR intensity, since the production of one photoelectron requires an energy deposition in the scintillator of about 4 keV. Because of this, the XTR photon detection efficiency in the richest part of the spectrum (5–10 keV) is 50–80%. Figure 17a shows the distributions of the energy deposition (experimental and calculated) in one of the scintillators for the detection of pions, kaons, and protons with energy 300 GeV. Although the measured distribution is shifted appreciably to the left compared with the expected distribution, and the authors of Ref. 62 have not yet explained this discrepancy, even in such a situation there is fairly good π/K identification. (By definition, a particle that in both XTR detectors produces a signal less than the threshold value is assumed to be a kaon). Figure 17b shows on an expanded scale the initial part of the energy-

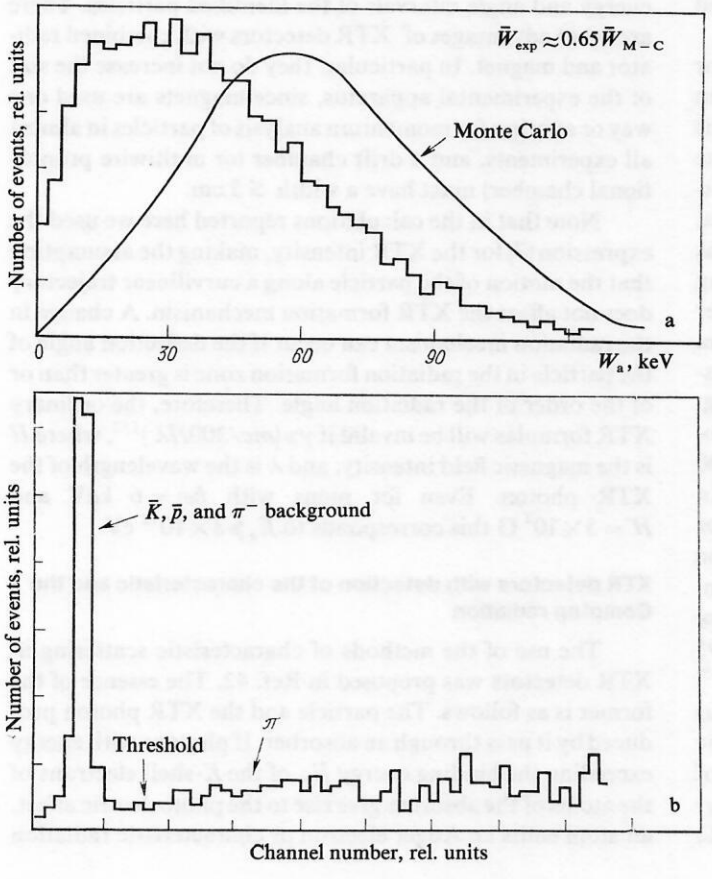

FIG. 17. Experimental (histogram) and calculated distributions of the XTR energy deposition in a scintillator[62] (a) and the initial part of the experimental XTR distribution in a scintillator (b).[62]

deposition distribution. Here, the events in the left-hand part are due to kaons, protons, and, depending on the threshold level, a certain fraction of the pions (background). If the discrimination level is in the neighborhoods of the single-photoelectron events (i.e., around 4 keV), then the contribution of the pions at $E = 300$ GeV is 0.19 (for ratio $\pi/K = 300/10$ in the original beam); but if the threshold is raised by just 20%, the pion fraction reaches 0.45. For comparison with Ref. 60, we mention that the pion detection efficiency was here 97% in each of the detectors, this corresponding to detection on the average of 3.5 photons. The authors of Ref. 62 express the hope that after elimination of the discrepancy between the calculated and measured radiation intensities the π/K identification will be greatly improved. It is readily estimated that for the given parameters of the radiator and the scintillator, detection of about six XTR photons is expected, and this will correspond to a pion detection efficiency of ~ 0.995, and their fraction in kaon events will not exceed 3%.

Although the XTR detectors using magnets described above have numerous indisputable advantages (high resolution and a very simple construction compared with multimodule energy-deposition XTR detectors), they do have two shortcomings. First, they measure the total energy of the XTR photons, and information about the number of photons is lost. The fluctuations in the energy of the detected photons are 100–200% (see Figs. 16b and 17a), appreciably greater than the fluctuations in the number of photons, which satisfy the Poisson distribution. Second, it is practically impossible to identify secondary particles in narrow jets, since the XTR photons from all particles are detected together in a restricted part of the radiation detector.

These shortcomings can be avoided if the XTR radiator is placed, not before the bending magnet, as was done in Refs. 60–62, but directly in the gap of the magnet. In this case, each photon will be emitted along the tangent to the curvilinear trajectory of the particle's motion in the magnetic field. In the radiation detector, placed behind the magnet, the coordinates of the points of absorption of the photons emitted by the particle will lie along the straight line joining the points to the coordinates of the particle before and after the deflection of the particle. As a photon detector, one can use the device described, for example, in Ref. 63. To illustrate the possibilities of such an XTR detector, we give Fig. 18, which shows the dependences of the pion, kaon, and proton rejection coefficients on the detection efficiency at 300 GeV. We made these calculations for a lithium radiator. In each case we optimized the parameters of the XTR detector appropriately. As can be seen from Fig. 18, the combination of the radiator with the bending magnet significantly improves the resolution of the XTR detector. Thus, in the case of the separation of pions from kaons at efficiency $\varepsilon_\pi = 0.95$ the rejection coefficient is expected to be $\delta_K \approx 5 \times 10^{-5}$. Moreover, a possibility is here opened up of simultaneous identification of pions, kaons, and protons. Namely, if the radiator parameters are optimized for the identification of kaons and protons (continuous curves) and if for the purposes of an estimate we take a detection efficiency $\varepsilon_K \approx 50\%$,

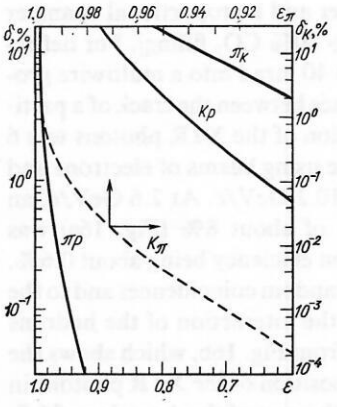

FIG. 18. Dependence of the rejection coefficient δ on the detection efficiency ε in $\pi/K/p$ identification (continuous curves) and π/K identification (broken curve).

then the contributions of the pions and protons are, respectively, $\delta_\pi \approx 8 \times 10^{-3}$ and $\delta_p \approx 10^{-3}$. (In Fig. 18, the values of ε and δ refer to the particles indicated on the curves first and second, respectively.) At higher energies of the particles, the resolution will be even higher.

Thus, a simple analysis of the number of detected XTR photons makes it possible to identify simultaneously pions, kaons, and protons with a fairly high efficiency and good rejection, i.e., such a device is a differential XTR detector. We use this name here by analogy with a differential Cherenkov counter, but, in contrast to the latter, an XTR detector can work without readjustment of the parameters in wide energy and angle intervals of the identified particles. There are other advantages of XTR detectors with combined radiator and magnet. In particular, they do not increase the size of the experimental apparatus, since magnets are used one way or another for momentum analysis of particles in almost all experiments, and a drift chamber (or multiwire proportional chamber) must have a width $\lesssim 5$ cm.

Note that in the calculations reported here we used the expression (7) for the XTR intensity, making the assumption that the motion of the particle along a curvilinear trajectory does not affect the XTR formation mechanism. A change in the radiation mechanism can occur if the deflection angle of the particle in the radiation formation zone is greater than or of the order of the radiation angle. Therefore, the ordinary XTR formulas will be invalid if $\gamma \gg (mc/300H\lambda)^{1/2}$, where H is the magnetic field intensity, and λ is the wavelength of the XTR photon. Even for pions with $\hbar\omega = 6$ keV and $H = 5 \times 10^4$ G this corresponds to $E_\pi \gg 3 \times 10^{12}$ eV.

XTR detectors with detection of the characteristic and the Compton radiation

The use of the methods of characteristic scattering in XTR detectors was proposed in Ref. 42. The essence of the former is as follows. The particle and the XTR photon produced by it pass through an absorber. If photons with energy exceeding the binding energy E_K of the K-shell electrons of the atoms of the absorber give rise to the photoelectric effect, an atom emits an Auger electron or characteristic radiation

with energy $\hbar\omega \approx E_K$. The absorption coefficient of the latter in the absorber itself is several times less than for the primary photon, and its direction is isotropic. Therefore, photons of the characteristic radiation can be detected in directions different from that of the particle's motion. Namely, it was an XTR detector of this type that was used in an experiment to measure the horizontal flux of cosmic-ray muons at energies $\geqslant 700$ GeV.[64] In this experiment, a xenon absorber of thickness 10 cm was placed directly behind an XTR radiator (300 layers of paper, $a = 200\ \mu$m, $b = 1$ cm). The characteristic radiation was detected by means of eight NaI(Tl) scintillators placed above and below the absorber. In this experiment, the efficiency of XTR particle detection was low, about 12%. It was in this experiment that x-ray transition radiation was observed for the first time.

A much higher efficiency was achieved in the XTR detector of Ref. 65, in which the radiator was placed directly in an absorber gas (krypton), and the characteristic radiation was detected by means of 16 CsI(Tl) scintillators placed on both sides of the radiator. This last had transverse dimensions 3×3 cm and consisted of 1300 layers of mylar with thickness 10 μm and separated by 280 μm. To eliminate the background from random coincidences, only particles whose passage through the radiator was accompanied by the detection of $n > 3$ characteristic photons were selected. An electron detection efficiency of about 30% was achieved, and if it had been possible to realize the detection condition $n \geqslant 1$, the efficiency would have been approximately 85%. The improvement in the efficiency compared with Ref. 65 was a consequence of a more rational choice of the absorber gas and the radiator parameters, as well as of the placing of the radiator directly in the absorber gas. This reduced the fraction of XTR photons absorbed in the radiator itself and greatly increased the probability of their absorption in the absorber gas.

To separate the XTR photons from the particle that has produced them, one can also use the processes of coherent and Compton scattering of these photons in the materials of the radiator or in an absorber placed behind it. Such XTR detectors were investigated in Refs. 66–69. In particular, a device in which the radiator was surrounded by ten proportional counters whose anode wires were stretched along the detector axis was investigated in Refs. 66–68. Polypropylene of density 0.04 g/cm^3, diameter 6 cm, and length 190 cm was used as a radiator (and, simultaneously, as a radiation scatterer). For comparison, an investigation was also made of a radiator in which a copper foil of thickness 6 μm (in which the characteristic radiation was produced) was placed after every 2 cm of the polypropylene. The measurements showed that the methods of detection of the characteristic radiation and the Compton scattering had much the same efficiency. A common shortcoming of both methods is the restriction which they impose on the transverse dimensions of the XTR detector—with increasing transverse dimensions of the radiators (or absorbers) the probability of absorption of the secondary radiation increases strongly. As follows from the calculations given in Ref. 68, an increase in the diameter of the radiator from 6 to 50 cm reduces the number of detected photons by a factor 1.5–2 for a particle that passes along the radiator axis. The numbers of photons for a particle passing along the axis of a radiator of diameter 50 cm and at a distance of 20 cm from it differ by a factor 1.5.

Method of angular discrimination

For separate detection of the particle and the radiation, one can exploit the features of the angular distribution of x-ray transition radiation. It was shown in Ref. 70 that, depending on the value of γ, the number of emitted photons can change strongly in a given angular interval 0–θ. In particular, if $\theta^2 \gg \gamma^{-2}$, the radiation intensity has a logarithmic dependence on γ. In the interval $\theta^2 \ll \gamma^{-2}$, this dependence is much steeper, and the intensity is very low:

$$\frac{dW}{d\omega} \approx \frac{e^2}{\pi c}\left(\frac{\sigma\gamma^2}{\omega^2+\sigma\gamma^2}\right)^2 \theta^4\gamma^4. \qquad (17)$$

And if particles with masses $m_1 < m_2$ are identified, then, using a detector of toroidal shape, one can, by choosing its diameter and the distance to the XTR radiator appropriately, satisfy simultaneously the conditions $\theta_2^2 \gtrsim \gamma_1^{-2} \gg \theta_1^2$ and $\gamma_2^{-2} \gg \theta_2^2 \gg \theta_1^2$ (θ_2 and θ_1 are the angles subtended by the outer and inner radii of the radiation detector). The inner opening of the torus is intended to let through the charged particles. In the experiment of Ref. 71, the energy dependence of the detected radiation intensity increased with decreasing angular interval. For electrons with energies 0.5–3.0 GeV and for $\theta_1 = 2.6\times 10^{-4}$ and $\theta_2 = 2.5\times 10^{-3}$, the energy dependence has the form $E^{2.2}$. At the same time, the electron detection efficiency was low, about 10%. Although subsequently a project for such a device was proposed for the separation of muons with energies 100–200 GeV,[72] it is obvious that such XTR detectors can be used only to tag light particles in well-collimated beams.

In Ref. 73, a study was made of an XTR detector based on the energy-deposition method in which the angular distribution of the x-ray transition radiation was used as a second criterion to raise the resolution. At a certain distance from the radiator, a drift chamber was placed to detect not only the particle but also the XTR photons. The electronics made it possible to measure both the total charge Q produced in the chamber and the width W of its spatial distribution (i.e., the drift time). It is obvious that for particles not accompanied by x-ray transition radiation Q and W will be less than the corresponding quantities for a particle that is. Figure 19 gives the pion rejection coefficient as a function of the kaon detection efficiency in the case of analysis of Q alone (energy-deposition method) and also in the case of simultaneous analysis of Q and W. The results were obtained for one module of an XTR detector consisting of a lithium radiator ($a = 30\ \mu$m; $b = 300\ \mu$m, $n = 1500$) and a drift chamber of thickness 8 mm and filled with a 60% Xe + 40% CO_2 mixture and then converted to a 15-module XTR detector. As follows from Fig. 19, the use of the angular distribution as a second criterion raises the resolution by 4–4.5 times. However, the length of the XTR detector is also greatly increased, and a 15-module detector with the parameters given above will have a length of 10–12 m.

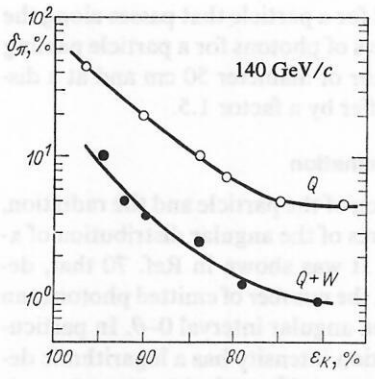

FIG. 19. Dependence of the pion rejection coefficient on the efficiency of kaon detection by the total energy-deposition method with allowance ($Q + W$) and without allowance (Q) for the width of the spatial distribution of the clusters.[73]

Streamer-chamber method

In 1970, the use of a streamer chamber was proposed[74] for separate detection of x-ray transition radiation and the particle that had produced it. In the chamber, one can trace visually quite clearly the chain of clusters along the particle track produced by the δ electrons, and also the individual clusters around the track due to the absorbed XTR photons. If a bending magnet is used between the radiator and the streamer chamber, the clusters formed by the photoelectrons are more clearly distinguished. It is obvious that the visual and electronic[51,53,54] methods of cluster detection do not differ in principle. Nor should in practice the resolutions of the XTR detectors using these two methods. Although the electronic method of counting the number of clusters has undoubted advantages over the steamer-chamber method, we shall briefly consider the results obtained by means of the latter.[74–78] In the quoted studies, the XTR radiator was mainly polypropylene ($\rho = 0.04$ g/cm^2, $\bar{a} = 14\,\mu$m, $b = 200\,\mu$m) of different lengths. The streamer chamber had length 80 cm along the particle track; it was filled with a (74–87)% Ne + (26–13)% Xe mixture. The measurements were made at electron energies 1.3–4.5 GeV.

Figure 20 shows the experimental distributions of the cluster number at the electron energies 1.3 and 4.5 GeV when a bending magnet was used (the histograms corresponding to Poisson distribution with mean numbers of clusters 1.87 and 3.8 were calculated by the present author). These distributions were obtained for a radiator of length 160 cm and a xenon concentration in the streamer chamber of 20%. If the distributions in Fig. 20 are ascribed to kaons and pions, respectively, and if events with a number of clusters $\geqslant 3$ are selected, then the pion detection efficiency is 43% with a kaon rejection coefficient of about 0.12. It is obvious that to improve the resolution of the XTR detector, it is necessary to use seveal modules, and this is very complicated in the case with a bending magnet. Therefore, the authors of Ref. 78 considered the possibility of creating a multimodule system without bending magnets. It follows from their estimates deduced from the results of measurements with a single-module XTR detector that in a system of 20 chambers (each of length 20 cm, 26% Xe + 74% Ne filling)

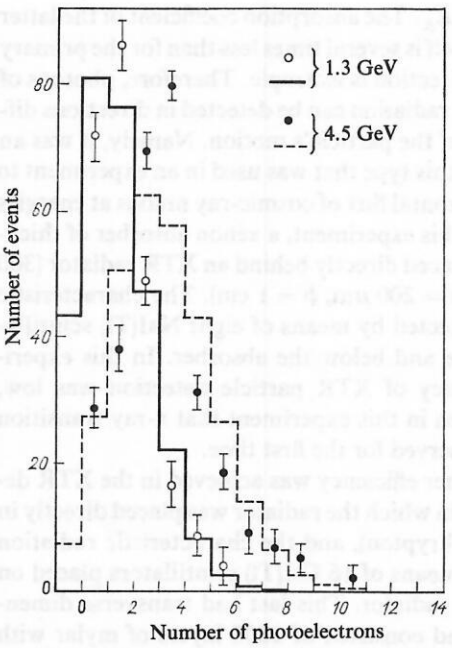

FIG. 20. Distribution of the number of photoelectrons detected in the streamer chamber (the open circles and black circles correspond to the experiment of Ref. 78, and the histograms to the calculations).

and radiators of length 20 cm, each will detect about 13 and 25 XTR photons, respectively, at the electron energies 1.0 and 3.75 GeV. At the same time, the number of detected δ electrons at both energies will be 17. This is equivalent to detection on the average of 30 and 42 clusters, respectively, in the identification of 270-GeV kaons and pions. However, the following should be noted. Judging from the number of δ electrons, the cluster detection threshold here corresponds to an energy of the δ electrons of about 3 keV. Comparing the numbers of δ electrons per unit amount of matter that are detected under the conditions of the experiments of Refs. 54 and 78, we find that in the latter it is lower by approximately a factor of 2, although the cluster detection threshold in Ref. 54 corresponds to 4 keV. At the same time, the number of δ electrons detected in Ref. 54 is fairly close to the expectation.

3. EXPERIMENTS USING XTR DETECTORS

As already mentioned, the first attempt to use XTR detectors was made as early as 1964 in an experiment to measure the energy spectrum of muons of the horizontal cosmic-ray flux with energies $\geqslant 700$ GeV.[64] Ten years later, the possibility of combining an XTR detector with an ionization calorimeter for the identification of cosmic-ray pions and protons with energies $\geqslant 300$ GeV was tested.[79] During the following years, several experiments using XTR detectors were realized. Below, we shall review these experiments.

In Refs. 80–82 there is a description of the apparatus and the main results of an experiment to investigate the composition of the hadron component of the cosmic rays at 2900 m above sea level and to measure the cross section for the interaction of pions and protons with iron nuclei at energies $\geqslant 400$ GeV. The arrangement of the experiment is shown in Fig. 21a. The ionization calorimeter, of area 4 m^2, is for the

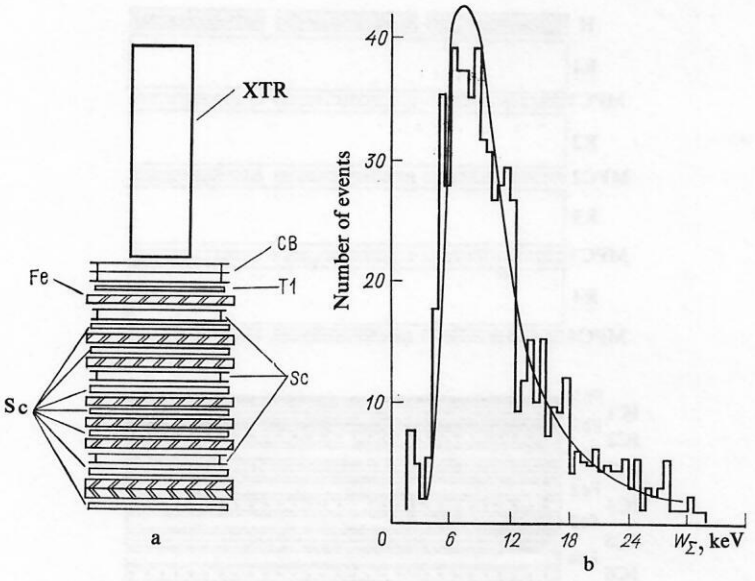

FIG. 21. Arrangement of experiment[80] (CB and SC are, respectively, two- and one-section wide-gap spark chambers; T1 and Sc are scintillation counters of the telescope and calorimeter, respectively; Fe shows the iron layers) (a) and comparison of the calibration distribution of the energy deposition in the case of a porous material (histogram) with the calculated equivalent laminated radiator (continuous curve) (b).

measurements of the hadron energy. It consists of eight layers of iron each of thickness 15 cm. Between the layers are scintillation counters S1–S7 and wide-gap spark chambers SC1–SC3. The scintillation counters T1 and T2 together with the counters S1–S7 make it possible to detect events due to hadrons that do not have a dense air accompaniment. Isolated hadrons were separated by means of the spark chamber SCB. The XTP detector, of area 1 m^2 and placed above the central part of the calorimeter, consists of 24 modules. The multiwire proportional chambers of the modules of the XTR detector are 5-cm wide and filled with a 90% Ar + 10% CH_4 mixture; one signal is taken from each proportional chamber. They were calibrated by radioactive sources, muons, and also hadrons with energy $\geqslant$100 GeV. The radiators were made of Dow Styrofoam, each 13.6-cm thick. On the basis of the results of Ref. 23 it was shown that 4 cm of such polypropylene corresponds in its radiation capacity at $\gamma = 2600$ to a laminated medium with $a = 17.5\,\mu$m, $b = 750\,\mu$m, $n = 31$ (Fig. 21b). For such an equivalent laminated medium, the Monte Carlo method was used to obtain the mean values of the energy deposition $\bar{W}_a$ at $\gamma = 2000$, 3600, and 5600. With an error of 10%, these values agreed with the results of the calibration of the polypropylene radiator in the electron accelerator at the same values of γ. Therefore, all the subsequent analysis of the experimental results was based on Monte Carlo calculations with the foregoind parameters of the equivalent laminated medium. It should be noted that the equality of the $\bar{W}_a$ values of the porous and periodic radiators at three values of γ in no way means that their distributions will coincide in the complete range $4\times10^2 \leqslant \gamma \leqslant 1.5\times10^4$.

For identification, 375 isolated hadrons corresponding to the following criteria were selected: The hadron trajectory must pass through $\geqslant$10 modules; if there is an albedo particle that leaves the calorimeter and enters the upper hemisphere, then the readings of the last three of the multiwire proportional chambers situated along the trajectory of the identified particle are rejected. Figure 22 shows the distribution of the energy depositions of all selected hadrons with energy $\geqslant$400 GeV in the proportional chambers of one module; for comparison, we give the analogous distribution for hadrons with energies $90 \leqslant E \leqslant 150$ GeV. Since protons even with energies $400 \leqslant E \leqslant 1000$ GeV hardly produce transition radiation, the authors of the experiment naturally attributed the difference between the distributions to the presence of a certain fraction of pions among the high-energy hadrons. The ratio N_π/N_p of the number of pions to the number of protons was determined by statistical analysis using the method of maximal likelihood [see (14) and (15)]. The values of $P^i_\pi(W)$ and $P^i_p(W)$ were determined from the calculated distributions. Figure 33a shows the distribution of R for 300 hadrons

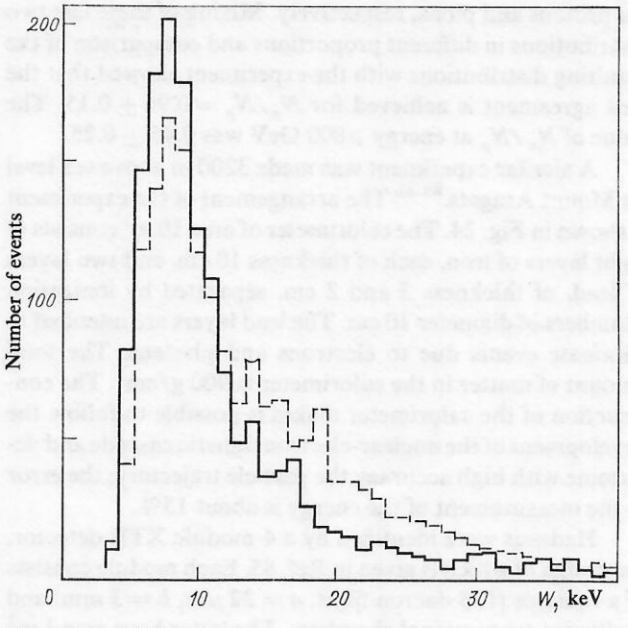

FIG. 22. Distributions of the energy deposition in one multiwire proportional chamber of hadrons with energies $90 \leqslant E \leqslant 150$ GeV (continuous histogram) and $E \geqslant 400$ GeV (broken histogram).

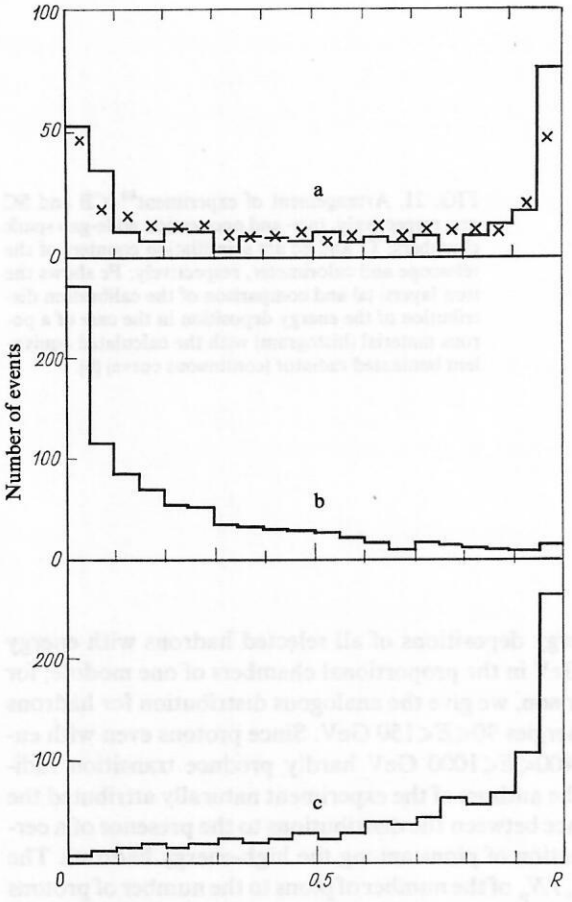

FIG. 23. Distributions of R for hadrons with energies $400 \leqslant E < 800$ GeV (experiment) (the crosses correspond to the calculation for $N_\pi/N_p = 0.96 \pm 0.15$) for protons (calculation) and for pions (calculation).

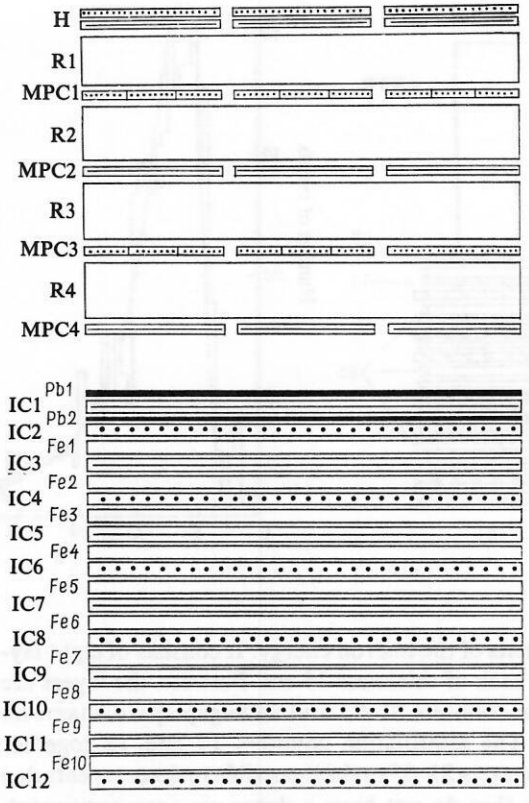

FIG. 24. Arrangement of experiment[83] (H is the hodoscope, R is the radiator, Pb and Fe are layers of lead and iron, respectively, and IC are ionization chambers).

with energy $400 \leqslant E \leqslant 800$ GeV detected in the experiment, and Figs. 23b and 23c give the calculated distributions of R for protons and pions, respectively. Mixing of these last two distributions in different proportions and comparison of the resulting distributions with the experiment showed that the best agreement is achieved for $N_\pi/N_p = 0.96 \pm 0.15$. The value of N_π/N_p at energy $\geqslant 800$ GeV was 0.45 ± 0.25.

A similar experiment was made 3200 m above sea level on Mount Aragats.[83–86] The arrangement of the experiment is shown in Fig. 24. The calorimeter of area 10 m^2 consists of eight layers of iron, each of thickness 10 cm, and two layers of lead, of thickness 3 and 2 cm, separated by ionization chambers of diameter 10 cm. The lead layers are intended to eliminate events due to electrons and photons. The total amount of matter in the calorimeter is 900 g/cm^2. The construction of the calorimeter makes it possible to follow the development of the nuclear-electromagnetic cascade and determine with high accuracy the particle trajectory; the error in the measurement of the energy is about 15%.

Hadrons were identified by a 4-module XTR detector, the design of which is given in Ref. 85. Each module consists of a radiator (125 dacron films, $a = 22$ μm, $b = 3$ mm) and multiwire proportional chambers. The latter have area 1 m^2 and effective thickness 2.9 cm; the filling is 90% Ar + 10% C_3H_8. Each multiwire proportional chamber is divided into three sections, and their directions in successive modules are mutually perpendicular, this making it possible to reduce effectively the background of the air accompaniment and the albedo particles. The proportional chambers were calibrated by radioactive sources, low-energy hadrons, and cosmic-ray muons. The equipment detected events if the energy released in the calorimeter was $\geqslant 300$ GeV and the nuclear-electromagnetic cascade covered at least four layers of iron.

Altogether, 3200 hadrons (isolated or with low-density accompaniment) were selected and analyzed. The method of maximal likelihood was used to analyze the information from the XTR detector. In the energy intervals $300 \leqslant E < 500$ GeV, $500 \leqslant E < 1000$ GeV, and $E \geqslant 1000$ GeV the ratio N_π/N_p was found to have the values 0.93 ± 0.15, 0.40 ± 0.12, and 0.08 ± 0.05, respectively, in good agreement with the results of Ref. 82.

It is of interest to compare the studies of Refs. 85 and 81. There is a striking difference between the numbers of modules of the XTR detector: four and 24; as follows from Ref. 81, a particle trajectory covered on the average 12 modules of the latter. In addition, the polypropylene of thickness 13.6 cm used in Ref. 81 as a radiator is equivalent to 50 or 60 dacron layers, whereas in Ref. 85 each radiator contained 125 dacron layers. As a result, at high energies the resolutions of the two devices hardly differed at $\varepsilon_\pi \approx 60\%$. At lower energies, the resolution in Ref. 81 was better than in Ref. 85, although in the latter δ_p still remained at the level of 10%. But at the same time the use in Ref. 85 of four modules

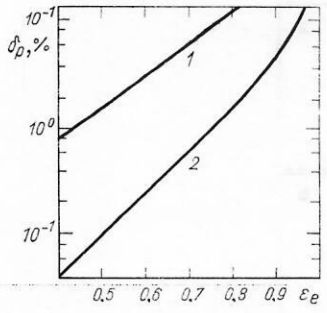

FIG. 25. Proton rejection coefficient δ_p as a function of the electron detection efficiency ε_e at $\gamma = 500$ (curve 1) and $\gamma = 2\times10^4$ (curve 2).

made it possible to increase appreciably the transverse dimensions of the equipment and, therefore, the rate of accumulation of statistics. This, in its turn, made it possible, when necessary, to reduce the particle detectoin efficiency and raise the resolution of the XTR detector.

Another field of application of XTR detectors is to the separation of electrons from hadrons. It would seem that this can be done much more readily than the separation of pions from protons, since at a given energy the Lorentz factors of the identified particles differ, not by seven times, as in the case of π/p separation, but by hundreds and thousands of times. Indeed, in accelerators in which the energy interval is limited, electrons and hadrons can be identified comparatively easily. However, in cosmic-ray experiments, where the energies are effectively unlimited, and $N_e/N_p = 10^{-2}$–10^{-3}, the separation of the particles is much more difficult. Nevertheless, the first experiment using an XTR detector to separate electrons and protons was made with the aim of measuring the differential electron spectrum of the primary cosmic rays in the region of energies 10–200 GeV.[87,88] The experimental equipment consisted of a shower detector, a transition-radiation detector, and a scintillation telescope. The shower detector contained three layers of lead with thicknesses equal to 4, 2, and 3 radiation units of length and scintillation counters. It was designed to separate protons and electrons and to measure the energies of the latter. However, although the thickness of the shower detector was taken to be much less than the proton interaction range, the number of detected protons, which masked the electrons, was still fairly large, since $N_e \ll N_p$. In this case, it was necessary to reduce the proton rejection coefficient by a further factor of 10^2–10^3. This was done by an XTR detector containing six modules. Each of them consisted of a radiator (Dow Ethafoam of density 0.037 g/cm^2 and thickness 14.5 cm) and a multiwire proportional chamber of thickness 2 cm, filled with an 80% Xe + 20% CO_2 mixture. Figure 25 shows the rejection coefficient δ_p as a function of the electron detection efficiency ε for $E \leqslant 500$ GeV and $E = 10$ GeV in such an XTR detector.[36] Events due to electrons were identified by calculating the maximal-likelihood parameter [cf. (15)]

$$L = \prod_{i=1}^{6} P_e^i(W) / \prod_{i=1}^{6} P_p^i(W); \tag{18}$$

it was assumed that an event is due to an electron if $L \gg 1$, or to a proton is $L \ll 1$, and is unidentifiable if $L \sim 1$. Figure 26a shows the L distribution, from which it follows that the electrons can be well discriminated from protons. Figure 26b gives the differential spectra of the electrons of the primary cosmic rays measured in the experiment (points) and averaged over the known experiments made up to 1975 (continuous line). It can be seen that the spectrum measured in Ref. 88 is appreciably steeper than that which follows from the early experiments. The authors state that the measured spectrum corresponds to an age $\sim 10^7$ yr of the galactic cosmic rays.

An interesting experiment was made with an XTR detector at the CERN Intersecting Storage Ring to study the production of e^+e^- pairs with invariant mass $\gtrsim 2.5$ GeV/c^2.[89,90] The arrangement of the experiment is shown in Fig. 27. It consists of a liquid-argon calorimeter, hodoscope scintillators, and a two-module XTR detector. The calorimeter ensures a highly accurate measurement of the energy of the particles and also, with rejection coefficient $\sim 2\times10^{-3}$, reduces the hadron background (the electron detection effi-

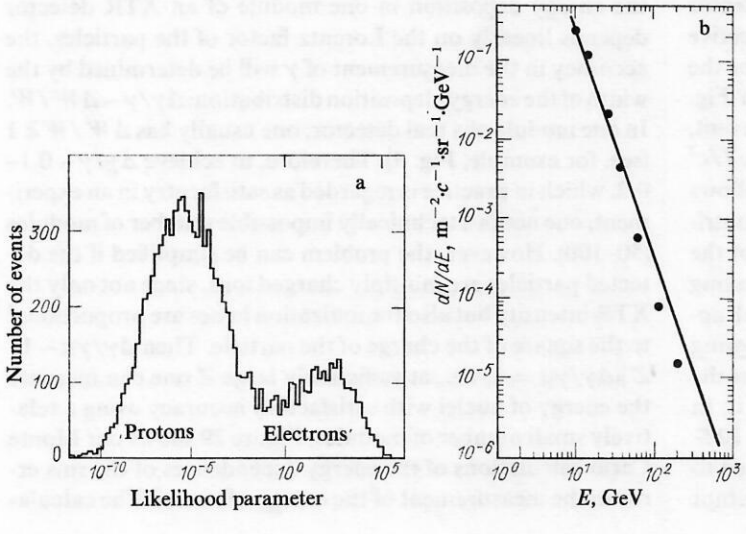

FIG. 26. Distribution of the likelihood parameter[87] (a) and differential electron spectrum of primary cosmic rays (b).

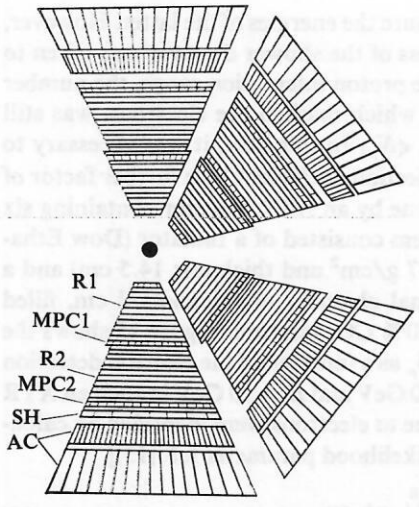

FIG. 27. Arrangement of experiment[89]: R denotes a radiator, SH the scintillation hodoscope, and AC the liquid-argon calorimeter.

ciency being about 83%). A further suppression of the hadron background is achieved by the XTR detector ($a = 50$ μm, $b = 300$ μm, $n = 650$–700 layers). The minimal energy of the detected electrons was 700 MeV, and since at such energies it is mainly soft transition-radiation x rays that are emitted, the radiator was made of lithium foils to reduce the absorption of the x rays in the radiator itself. Multiwire porportional chambers of thickness 1.3 cm and filled with 80% Xe + 20% CO_2 were used to detect the radiation. In them, the readout was from each wire separately. The charge-division method was used in them,[93] and this made it possible not only to determine the trajectories in the XTR detector but also to identify several particles simultaneously. Investigations in pion and electron beams showed that the combination of lithium radiators with such proportional chambers ensured a pion rejection coefficient not worse than 8×10^{-2} with electron detection efficiency 60–90% in the energy interval 0.75–4.0 GeV.[25,91,92]

Figure 28 shows the distribution of the effective masses of the electron-positron pairs measured in the experiment of Ref. 89; after the hodoscope reading has been taken into account, an appreciable fraction of them were rejected (Fig. 28b). After the rejection of the hadrons by the XTR detector (Fig. 26b), a clear peak appeared in the region of effective mass ~3 GeV/c^2. The final analysis with allowance for the calorimeter readings led to the distribution shown in Fig. 28d. Thus, form more than 10^4 candidates for a J/ψ event, just 93 events with effective mass $2.7 < m_{e^+e^-} < 3.4$ GeV/c^2 that met all the selection criteria were chosen. As follows from Fig. 28d, the XTR detector made an important contribution in this selection. In the process of calibration of the XTR detector and its use in the experiment, an interesting detail was noted—in 30–40% of the events, a signal appeared in the multiwire porportional chambers following normal incidence of electrons not only at the point on the particle trajectory but also at a certain distance from it; in the case of pion detection, such events were observed in 10% of the cases. In Ref. 89, this phenomenon was attributed to Compton scattering of the XTR photons, and an attempt

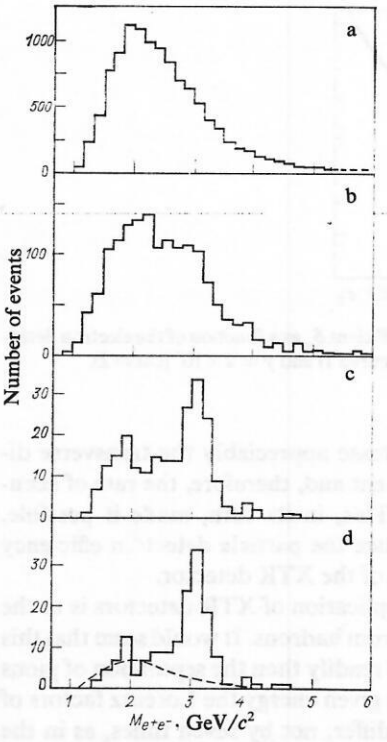

FIG. 28. Effective-mass distribution: a) the original; b) after correction for the scintillation-hodoscope readings; c) the same after allowance for electron identification by the XTR detector; d) the same after the final analysis of the results. The broken curve shows the background contribution.

was made to use it as an additional factor in improving the rejection coefficient of the XTR detector. However, subsequent investigations showed that in the case of inclined incidence on the multiwire proportional chambers the pions also produced with high probability an additional signal far from the particle track. Therefore, it was not possible to use Compton scattering to improve the resolution of the XTR detector.

Hitherto, we have considered experiments in which XTR detectors were designed to identify particles of different species but with known energy. Immeasurably more difficult is the problem of measuring the energy (or rather, γ) of particles with known mass. Indeed, even if it is assumed that the energy deposition in one module of an XTR detector depends linearly on the Lorentz factor of the particles, the accuracy in the measurement of γ will be determined by the width of the energy-deposition distribution: $\Delta\gamma/\gamma \sim \Delta W/W$. In one module of a real detector, one usually has $\Delta W/W \gtrsim 1$ (see, for example, Fig. 9). Therefore, to achieve $\Delta\gamma/\gamma \sim 0.1$–$0.2$, which in practice is regarded as satisfacotry in an experiment, one needs a technically impossible number of modules (50–100). However, the problem can be simplified if the detected particles are multiply charged ions, since not only the XTR intensity but also the ionization losses are proportional to the square of the charge of the particle. Then $\Delta\gamma/\gamma)z \sim 1/Z)(\Delta\gamma/\gamma)z = 1$, i.e., at sufficiently large Z one can measure the energy of nuclei with satisfactory accuracy using a relatively small number of modules. Figure 29 shows our Monte Carlo calculations of the energy dependences of the rms error in the measurement of the energy of nuclei. The calcula-

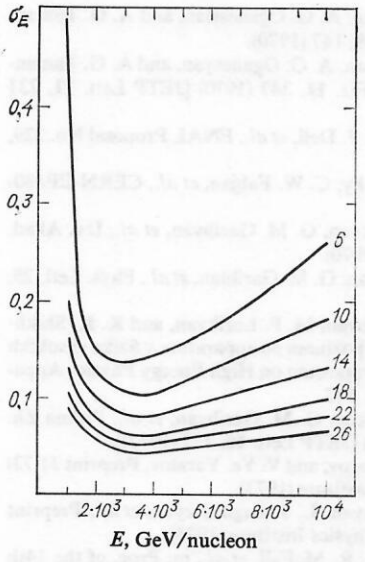

FIG. 29. Energy dependence of the rms error in the measurement of nuclei (the numbers next to the curves are the nuclear charges).

tions were made for a two-module XTR detector of mylar radiators and xenon multiwire proportional chambers ($a = 40\mu$m, $b = 500\mu$m, $n = 440$, $l_{Xe} = 5$ cm). It can be seen that already at $Z = 10$ the XTR detector is not inferior to calorimeters as regards the accuracy of the measurement.

At $E \gtrsim 100$ GeV/nucleon, the only source of multiply charged ions is cosmic rays outside the Earth's atmosphere. Therefore, proposals to use XTR detectors are asociated with the investigation of the energy spectra of nuclei of the primary cosmic rays.[94–96] However, we mention a serious technical problem that arises when energy-deposition XTR detectors are used to measure the energy of nuclei. It is known that at high ionization densities (as is the case in detection of nuclei) a large space charge arises in the gas of multiwire proportional chambers, and this leads to saturation of the gas multiplication.[97] This destroys the proportionality between the energy deposition in the gas and the siganl from the proportional chamber. In view of the wide range of detected W_Σ values (with allowance for fluctuations, $W_{Z=30}/W_{Z=4} \approx 10^3$), it is hard to believe that this problem can be avoided by the choice of the regime of operation of the proportional chamber. It is evident that the only possibility is to replace the multiwire proportional chambers by some other x-ray detector (for example, an ionization chamber).

The XTR detectors have undergone a long development; this process is still continuing. However, it is now obvious that among the known devices only they can ensure suitable resolution at superhigh energies. This circumstance, and also their simplicity, large transverse dimensions, and the ability to operate without readjustment in a wide range of energies provide the ground for the assertion that XTR detectors will be the main tool for identifying particles in experiments not only in the accelerators of the new generation but also in cosmic rays.

I am very grateful to Professor A. Ts. Amatuni and Professor G. A. Vartapetyan, who took the trouble to study the draft of this review, for valuable comments.

[1]V. P. Zrelov, Izluchenie Vavilova-Cherenkova i ego primenenie v fizike vysokikh énergiĭ (Cherenkov Radiaton and its Use in High Energy Physics), Vol. 2, Atomizdat, Moscow (1963).
[2]C. W. Fabjan and H. G. Fischer, Preprint CERN/80-27 (1980).
[3]I. M. Frank, Usp. Fiz. Nauk **75**, 231 (1961); **87**, 189 (1965) [Sov. Phys. Usp. **4**, 740 (1962); **8**, 729 (1966)].
[4]F. G. Bass and V. M. Yakovenko, Usp. Fiz. Nauk **86**, 189 (1965) [Sov. Phys. Usp. **8**, 420 (1965)].
[5]B. M. Bolotovskiĭ and G. V. Voskresenskiĭ, Usp. Fiz. Nauk **94**, 377 (1968) [Sov. Phys. Usp. **11**, 143 (1968)].
[6]M. L. Ter-Mikaelyan, Vliyanie sredy na élektromagnitnye protsessy pri vysokikh énergiyakh (Influence of the Medium on Electromagnetic Processes at High Energies), Armenian Academy of Sciences, Erevan (1969).
[7]S. M. Akhverdyan and G. M. Garibyan, Preprint EFI-339 (64)-78 [in Russian], Erevan (1979).
[8]A. I. Alikhanian, in: Proc. of the Fifth Intern. Conf. on Instrumentation for High Energy Physics, Frascati (1973), p. 350.
[9]A. I. Alikhanyan, in: Tr. Mezhdunar. simpoziuma po perekhodnomu izlucheniyu chastits vysokikh energiĭ (Proc. of the Intern. Symposium on Transition Radiation of High Energy Particles), Physics Institute, Erevan (1977), p. 41.
[10]L. A. Vardanyan and I. G. Melkumova, Bibliografiya rabot po perekhodnomu izlucheniyu 1945–1982 (Bibliography of Publications on Transition Radiation for 1945–1982), Physics Institute, Erevan (1983).
[11]V. L. Ginzburg and I. M. Frank, Zh. Eksp. Teor. Fiz. **16**, 15 (1946).
[12]G. M. Garibyan, Zh. Eksp. Teor. Fiz. **37**, 527 (1959) [Sov. Phys. JETP **10**, 372 (1960)].
[13]G. M. Garibyan, Izv. Akad. Nauk Arm. SSR, Fiz. **6**, 3 (1971).
[14]G. M. Garibyan and I. I. Gol'dman, Dokl. Akad. Nauk Arm. SSR **31**, 219 (1960).
[15]A. A. Avakyan, G. M. Garibyan, and C. Yang, Nucl. Instrum. Methods **128**, 601 (1975).
[16]A. A. Avakyan, G. M. Garibyan, and C. Yang, Nucl. Instrum. Methods **129**, 303 (1975).
[17]L. C. L. Yuan, C. I. Wang, H. Uto, and S. Prunster, Phys. Lett. **31B**, 603 (1970).
[18]A. A. Frangyan, F. R. Harutjunian, V. P. Kishinevski, *et al.*, in: Proc. of the Intern. Conf. for High Energy Physics, Dubna (1970), p. 530.
[19]R. Ellsworth, J. McFall, G. B. Yodh, *et al.*, in: Proc. of the 13th Intern. Conf. on Cosmic Rays, Denver (1973), p. 230.
[20]K. Hoshino, Y. Ohashi, A. Okada, *et al.*, in: Proc. of the 13th Intern. Conf. on Cosmic Rays, Denver (1973), p. 248.
[21]M. L. Cherry, G. Hartman, D. Müller, and T. A. Prince, Phys. Rev. D **10**, 3594 (1974).
[22]É. S. Belyakov, M. P. Lorikyan, K. Zh. Markaryan, and L. A. Gevorgyan, Preprint EFI-140(75) (1975).
[23]C. W. Fabyan and W. Struczinsky, Phys. Lett. **57B**, 483 (1975).
[24]M. L. Cherry and D. Müller, Phys. Rev. Lett. **38**, 5 (1977).
[25]J. Cobb, C. W. Fabyan, S. Iwata, *et al.*, Nucl. Instrum. Methods **140**, 413 (1977).
[26]C. W. Fabyan, Nucl. Instrum. Methods **146**, 343 (1977).
[27]M. L. Cherry, Phys. Rev. D **17**, 2245 (1978).
[28]A. A. Avakyan, M. P. Lorikyan, K. Zh. Markaryan, and Yu. L. Margaryan, see Ref. 9, p. 287.
[29]A. L. Avakyan, R. A. Astabatyan, L. A. Vardanyan *et al.*, Zh. Eksp. Teor. Fiz. **78**, 936 (1980) [Sov. Phys. JETP **51**, 471 (1980)].
[30]G. M. Garibyan and I. Ya. Pomeranchuk, Zh. Eksp. Teor. Fiz. **37**, 1828 (1959) [Sov. Phys. JETP **10**, 1290 (1960)].
[31]G. M. Garibyan and Shi Yan, Zh. Eksp. Teor. Fiz. **70**, 1627 (1976) [Sov. Phys. JETP **43**, 848 (1976)].
[32]G. M. Garibyan and Shi Yan, Izv. Akad. Nauk Arm. SSR, Fiz. **2**, 105 (1977).
[33]A. I. Alikhanian, K. M. Avakian, G. M. Garibyan, *et al.*, Phys. Rev. Lett. **25**, 635 (1970).
[34]H. Uto, L. C. L. Yuan, G. Dell, and C. L. Wang, Nucl. Instrum. Methods **97**, 389 (1971).
[35]A. I. Alikhanyan, E. S. Belyakov, and M. P. Lorikyan, Zh. Eksp. Teor. Fiz. **65**, 1330 (1973) [Sov. Phys. JETP **38**, 663 (1974)].
[36]T. A. Prince, D. Müller, G. Hartman, and M. L. Cherry, Nucl. Instrum. Methods **123**, 231 (1975).
[37]K. A. Ispiryan, S. A. Kankanyan, A. G. Oganesyan, and A. G. Tamanyan, Izv. Akad. Nauk Arm. SSR, Fiz. **7**, 377 (1972).
[38]C. W. Fabyan, in: Proc. of the Intern. Symposium on Transition Radiation of High Energy Particles, Erevan (1977), p. 256.
[39]A. I. Alikhanyan, E. S. Belyankov, *et al.*, Pis'ma Zh. Eksp. Teor. Fiz. **17**, 453 (1973) [JETP Lett. **17**, 325 (1973)].
[40]G. M. Garibyan, L. A. Gevorgyan, and Shi Yan, Izv. Akad. Nauk Arm.

SSR, Fiz. **8**, 248 (1973).
[41]G. M. Garibyan, L. a. Gevorgyan, and Shi Yan, Zh. Eksp. Teor. Fiz. **66**, 552 (1974) [Sov. Phys. JETP **39**, 265 (1974)].
[42]A. I. Alikhanyan, F. R. Arutyunyan, K. A. Ispiryan, and M. L. Ter-Mikaelyan, Zh. Eksp. Teor. Fiz. **41**, 2002 (1961) [Sov. Phys. JETP **14**, 231 (1961)].
[43]X. Artru, G. B. Yodh, and G. Menessier, Phys. Rev. D **12**, 1289 (1975).
[44]H. Fisher, S. Iwata, V. Radeka, *et al.*, Nucl. Instrum. Methods **127**, 525 (1975).
[45]M. L. Cherry, D. Müller, and T. A. Prince, Nucl. Instrum. Methods **115**, 141 (1974).
[46]C. Camps, V. Commichau, and M. Deutschman, Nucl. Instrum. Methods **131**, 411 (1975).
[47]A. T. Avundzhyan, A. G. Dadalyan, S. P. Kazaryan, and A. G. Oganesyan, Preprint EFI-492(35)-81 [in Russian], Erevan (1981).
[48]S. P. Kazaryan, S. A. Kankanyan, A. G. Oganesyan, and A. G. Tamanyan, Preprint EFI-103(75) [in Russian], Erevan (1975).
[49]A. G. Oganessian, A. T. Sarkissian, and M. Atac, Nucl. Instrum. Methods **145**, 251 (1977).
[50]K. A. Ispirian, S. G. Knyazian, and A. T. Margarian, in: Proc. of the Intern. Symposium on Transition Radiation of High Energy Particles, Erevan (1977), p. 209.
[51]R. A. Astabatyan, M. P. Lorikyan, G. A. Manukyan, and K. Zh. Markaryan, Preprint EFI-407(14)-80 [in Russian], Erevan (1980).
[52]R. A. Astabatyan, M. P. Lorikyan, and K. Zh. Markaryan, Izv. Akad. Nauk Arm. SSR, Fiz. **16**, 106 (1981).
[53]T. Ludlam, E. Platner, V. Polychronakos, *et al.*, CERN-EP/80-156 (1980).
[54]C. W. Fabjan, W. Willis, I. Gavrilenko, *et al.*, Nucl. Instrum. Methods **185**, 119 (1981).
[55]A. K. Drukier, C. Vallette, G. Waysand, *et al.*, Lett. Nuovo Cimento **14**, 300 (1975).
[56]A. K. Drukier, in: Proc. of the Intern. Symposium on Transition Radiation of High Energy Particles, Erevan (1977), p. 354.
[57]V. E. Pafomov, Dokl. Akad. Nauk SSSR **133**, 1315 (1960) [Sov. Phys. Dokl. **5**, 850 (1961)].
[58]L. A. Vardanyan, G. M. Garibyan, and Shi Yan, see Ref. 9, p. 374.
[59]B. Merkel, J. Repellin, G. Sauvage, *et al.*, Preprint LAL 1286, Universite Paris-Sud (1976).
[60]M. Bourqin, R. M. Brown, Y. Chatelus, *et al.*, Preprint CERN-EP/81-165 (1981).
[61]H. Stroble, University of Maryland Internal Report, August (1978).
[62]L. C. Myrianthopulos, R. E. Ellsworth, and R. G. Glasser, University of Maryland Internal Report, May (1980).
[63]A. Breskin, G. Charpak, and J. C. Santiard, Preprint CERN-EP/81-106 (1981).
[64]F. R. Arutyunyan, K. A. Ispiryan, and A. G. Oganesyan, Izv. Akad. Nauk SSSR, Ser. Fiz. **28**, 1866 (1964); Yad. Fiz. **1**, 842 (1965) [Sov. J. Nucl. Phys. **1**, 604 (1965)].
[65]A. I. Alikhanyan, K. A. Ispiryan, S. A. Kankanyan, *et al.*, Prib. Tekh. Eksp. **5**, 51 (1972).
[66]M. P. Lorikyan, Prib. Tekh. Eksp. **3**, 73 (1971).
[67]R. A. Astabatyan *et al.*, Prib. Tekh. Eksp. **2**, 75 (1980).
[68]A. L. Avakyan, R. A. Astabatyan, A. L. Vishnevskaya *et al.*, Izv. Akad. Nauk Arm. SSR, Fiz. **6**, 72 (1981).
[69]J. E. Mach, W. Z. Osborne, L. S. Pinsky, *et al.*, Phys. Rev. Lett. **33**, 1582 (1972).
[70]A. I. Alikhanian, K. A. Ispirian, A. G. Oganessian, and A. G. Tamanian, Nucl. Instrum. Methods **89**, 147 (1970).
[71]A. I. Alikhanyan, K. A. Ispiryan, A. G. Oganesyan, and A. G. Tamanyan, Pis'ma Zh. Eksp. Teor. Fiz. **11**, 347 (1970) [JETP Lett. **11**, 231 (1970)].
[72]P. W. Alley, A. Bamberger, G. P. Dell, *et al.*, FNAL Proposal No. 229, May (1973).
[73]M. Deutschman, W. Struczinsky, C. W. Fabjan, *et al.*, CERN-EP/80-155 (1980).
[74]A. I. Alikhanyan, K. M. Avakyan, G. M. Garibyan, *et al.*, Izv. Akad. Nauk Arm. SSR, Fiz. **5**, 267 (1970).
[75]A. I. Alikhanian, K. M. Avakian, G. M. Garibian, *et al.*, Phys. Lett. **25**, 635 (1970).
[76]A. I. Alikhanyan, G. M. Garibyan, M. P. Lorikyan, and K. K. Shikhlyarov, in: Tr. Mezhdunar. simpoziuma po apparature v fizike vysokikh énergiĭ (Proc. of the Intern. Symposium on High Energy Physics Apparatus), Vol. 2, Dubna (1971), p. 542.
[77]A. I. Alikhanyan, É. S. Belyakov, G. M. Garibyan, *et al.*, Pis'ma Zh. Eksp. Teor. Fiz. **16**, 315 (1972) [JETP Lett. **16**, 222 (1972)].
[78]M. P. Lorikyan, K. K. Shikhlyarov, and V. Ya. Yaralov, Preprint 31(73) [in Russian], Erevan Physics Institute (1973).
[79]A. I. Alikhanyan, V. V. Avakyan, L. S. Bagdasaryan, *et al.*, Preprint 100(74) [in Russian], Erevan Physics Institute (1974).
[80]R. W. Ellsworth, A. S. Uto, J. R. McFall, *et al.*, in: Proc. of the 14th Intern. Cosmic Rays Conf., Munich (1975), p. 2538.
[81]J. R. McFall, Ph.D. Thesis University of Maryland (1976).
[82]R. W. Ellsworth, A. S. Uto, J. R. McFall, *et al.*, in: Proc. of the 15th Intern. Conf. on Cosmic Rays, Vol. 4, Plovdiv (1974), p. 402.
[83]V. V. Avakyan, K. M. Avakyan, A. I. Alikhanyan, *et al.*, Izv. Akad. Nauk Arm. SSR Fiz. **38**, 1990 (1974).
[84]V. V. Avakian, A. T. Avunzhyan, K. G. Antonyan, *et al.*, in: Proc. of the 16th Intern. Conf. on Cosmic Rays, HE-4, Kyoto (1979), p. 61.
[85]A. T. Avundzhyan, S. P. Kazaryan, and A. G. Oganesyan, Preprint 437(44)-8) [in Russian], Erevan Physics Institute (1980).
[86]V. V. Avakian, A. T. Avundjian., L. S. Bagdasarian, *et al.*, in: Proc. of the 17th Intern. Conf. on Cosmic Rays, HE-3, 1-27, Paris (1981), p. 38.
[87]D. Müller, G. Hartman, and T. Prince, in: Proc. of the Intern. Symposium on Transition Radiation of High Energy Particles, Erevan (1977), p. 521.
[88]D. Müller, G. Hartman, and T. Prince, Phys. Rev. Lett. **38**, 1368 (1977).
[89]C. Kourkoumelis, CERN Report 77 (1976).
[90]W. Willis, in: Proc. of the Intern. Symposium on Transition Radiation of High Energy Particles, Erevan (1977), p. 243.
[91]J. H. Cobb, S. Iwata, R. B. Palmer, *et al.*, Phys. Rev. Lett. **72B**, 273 (1977).
[92]R. Bosshard, J. Fischer, S. Iwata, *et al.*, Nucl. Instrum. Methods **130**, 365 (1975).
[93]J. L. Arberi and V. Radeka, IEEE Trans. NS-23, 251 (1976).
[94]W. Z. Osborne and J. E. Mack, in: Proc. of the 14th Intern. Conf. on Cosmic Rays, Munich (1975), p. 3278.
[95]V. V. Avakyan, L. S. Bagdasaryan, S. P. Kazaryan, *et al.*, Preprint 177(23)-76 [in Russian], Erevan Physics Institute (1976).
[96]D. Müller and M. Cherry, in: Proc. of the Intern. Symposium on Transition Radiation of High Energy Particles, Erevan (1977), p. 137.
[97]U. Pollvogt and R. J. Kurz, IEEE Trans. NS-21, 1 (1974).

Translated by Julian B. Barbour